

Parameter estimation of structural dynamics with neural operators enabled surrogate modeling

Mingyuan Zhou^{a,b}, Haoze Song^c, Wenjing Ye^b, Wei Wang^{c,e}, Zhilu Lai^{a,d,*}

^aInternet of Things Thrust, The Hong Kong University of Science and Technology (Guangzhou), Guangzhou, China

^bDepartment of Mechanical and Aerospace Engineering, The Hong Kong University of Science and Technology, Hong Kong, China

^cData Science and Analytics Thrust, The Hong Kong University of Science and Technology (Guangzhou), Guangzhou, China

^dDepartment of Civil and Environmental Engineering, The Hong Kong University of Science and Technology, Hong Kong, China

^eDepartment of Computer Science and Engineering, The Hong Kong University of Science and Technology, Hong Kong, China

Abstract

Parameter estimation generally involves inferring the values of mathematical models derived from first principles or expert knowledge, which is challenging for complex structural systems. In this work, we present a unified deep learning-based framework for *parameterization*, *forward modeling*, and *inverse modeling* of structural dynamics. The parameterization is flexible and can be user-defined, including physical and/or non-physical (customized) parameters. In forward modeling, we train a neural operator for response prediction – forming a surrogate model, which leverages the defined system parameters and excitation forces as inputs. The inverse modeling focuses on estimating system parameters. In particular, the learned forward surrogate model (which is differentiable) is utilized for preliminary parameter estimation via gradient-based optimization; to further boost the parameter estimation, we introduce a neural refinement method to mitigate ill-posed problems, which often occur in the former. The framework’s effectiveness is verified numerically and experimentally, in both interpolation and extrapolation cases, indicating its capability to capture intrinsic dynamics of structural systems from both forward and inverse perspectives. Moreover, the framework’s flexibility is expected to support a wide range of applications, including surrogate modeling, structural identification, damage detection, and inverse design of structural systems.

Keywords: Inverse problems; parameter estimation; neural operators; structural dynamics; surrogate modeling.

1. Introduction

The study of physical systems generally comprises three fundamental steps [1]: Parameterization, forward modeling, and inverse modeling. The parameterization aims to discover a minimal set of parameters that fully characterize the investigated system. Subsequently, the forward modeling aims to make predictions on the system’s state, given values of system parameters and system inputs. Conversely, the inverse modeling involves estimating actual parameter values or other inputs of the system using some measurements of its state. These methodological steps have been foundational in addressing diverse problems in science and engineering. In this work, we draw inspiration from these steps and endeavor to integrate them with deep learning schema for structural dynamics applications.

In structural dynamics application, many sub-fields and tasks rely on effective modeling of structural systems [2]. For instance, forward modeling and inverse modeling are essential for *system identification* [3, 4] and *structural health monitoring* [5, 6], which are discussed in Section 2.2. Specifically, structural *response prediction* [7] focuses on predicting how structures will respond to external loading and initial/boundary conditions, which is viewed as forward modeling. Conversely, physical *parameter estimation* [8, 9] is inverse modeling, which seeks to determine the values of structural parameters, such as stiffness and damping coefficients. Similarly, *force identification* [10, 11] in mechanical or civil structures belongs to inverse modeling, which aims to infer the external forces acting on the

*Corresponding author. E-mail address: zhilulai@ust.hk

structures from the dynamic response measurements. Overall, building accurate mappings between excitation force, system parameters, and dynamic response is vitally important for structural dynamics applications.

The approaches of modeling structural dynamics generally fall into two streams: *solving-based* (model-based, first principles) approaches and *learning-based* (data-driven) approaches. In the solving-based methods [12, 13], mathematical models of structural systems are typically derived from first principles. Particularly, continuous structures are generally represented by partial differential equations (PDEs). The structural state is then determined by solving these PDEs analytically or numerically. Nevertheless, model-based methods can be challenging and computationally expensive for complex or realistic structural systems with unknown mechanisms.

In contrast, learning-based methods aim to model structural dynamics by closely capturing major dynamics directly from measured data, without necessarily requiring prior knowledge of structures. A comprehensive review of learning-based methods in structural dynamics can be found in [14]. Among various methods, machine learning models [15] such as multi-layer perceptron [16], autoencoder [17], convolutional neural networks [18], and physics-informed neural networks [19] have been extensively applied in structural dynamics. More recently, neural operators have emerged as powerful tools for solving PDEs in diverse fields [20–24], as introduced in Section 2.1. In structural dynamics, neural operators [25–27] have demonstrated improved response prediction performance compared to standard neural networks. However, most works focus on the forward modeling of structural dynamics, while the jointly forward and inverse modeling of structural dynamics is less explored in learning-based methods.

The two streams of approaches are not mutually exclusive but rather represent the different *prior* information used to address structural dynamics problems. In this work, we focus on the *learning-based* approaches to model structural dynamics. As many existing models focus on forward and inverse modeling separately, we hypothesize that they are strongly related and can be effectively addressed within a unified framework – a well trained forward surrogate model often leads to more accurate inverse parameter estimation. Additionally, deep learning models often learn structural system parameters implicitly with trainable weights. Developing learning-based methods that can estimate system parameters via neural networks remains an open, challenging problem in structural dynamics.

Recent progress in deep learning provides potential solutions for inverse modeling in structural dynamics. Researchers have explored neural networks in solving inverse problems, such as inverse design [28, 29], parameter estimation [30, 31], initial/boundary conditions estimation [32, 33], etc. A typical workflow involves first learning a neural surrogate model to approximate forward physical dynamics [32], and then performing back-propagation to optimize the input parameters of interest. As highlighted in [21, 31], deep learning models offer a promising technique for solving inverse problems.

Inspired by these deep learning approaches, to the best of our knowledge, this work pioneers to integrate the steps of parameterization, forward modeling, and inverse modeling with deep learning architectures and optimization techniques for structural dynamics applications. More specially, the contributions of this work are as follows:

- We propose a unified deep learning-based framework for modeling structural dynamics (Section 3.1), beginning with the parameterization of structural systems. The parameterization is flexible, that can include physical (Section 4.2.1) and/or non-physical (customized) (Section 4.3.1) parameters. The system parameters are subsequently utilized as input to the forward surrogate model for supervised training.
- Within this framework, we train a neural network as the surrogate model for forward modeling (Section 3.3.1). Specifically, we introduce a variant of the deep operator networks (AE-DeepONet), with its sub-modules specially designed for structural dynamics application, which merges excitation forces and system parameters to predict dynamic responses at one or multiple locations.
- In the inverse modeling (Section 3.3.2), we perform parameter estimation using *gradient-based initialization* on the learned forward surrogate model. To address potential inaccuracies in this initialization, we employ *neural refinement* to further boost the performance of parameter estimation. Ultimately, the inverse modeling offers a more complete data-driven solution for modeling structural dynamics.

The effectiveness of the framework is verified through a numerical Duffing oscillator and an experimental wind turbine blade. Notably, both interpolation and extrapolation test cases are considered to comprehensively evaluate the proposed framework.

2. Related works

2.1. Neural operators

Recently, considerable efforts have been dedicated to developing neural networks to learn operators from data [20–24], which map input function spaces to output function spaces. Lu et al. [20] propose the deep operator networks (DeepONet), which employ a branch-trunk architecture that is based on the universal approximation theorem of operators [34]. Li et al. [23] introduce the Fourier neural operator, which parameterizes a general convolutional operator to approximate nonlinear operators using the fast Fourier transform. Additionally, many other neural architectures such as graph neural operators [35], multi-grid neural operators [24], laplacian neural operators [22] have also been proposed, exhibiting improved generalization performance for solving partial differential equations than standard neural networks.

Neural operators are more natural solutions to learn structural dynamics from data, considering that the underlying mechanism of solving structural dynamics is applying certain operators. For instance, Garg et al. [36] use DeepONet to predict the displacement of dynamical systems under stochastic excitation force. Cao et al. [37] employ different neural operators to predict the structural responses of the floating structures under irregularly driven waves, which can be viewed as varying excitations. Additional studies [25–27] have explored the use of DeepONet to predict the response of dynamical systems with different initial conditions and input functions.

Previous research mainly investigates the response prediction of dynamical systems under varying excitations, and our work considers structural response prediction given varying system parameters – learning a family of operators other than a specific one. More importantly, we integrate the trained operators to serve for the parameter estimation in the framework – an open and challenging problem that is less addressed for neural network-based methods.

2.2. Structural system identification and health monitoring

Structural system identification is essential in understanding structural systems, which aims to develop models based on the input and/or output measurements from the investigated system. Extensive research has been conducted for nonlinear systems [3, 4], which typically involve three main steps: detection, characterization, and parameter estimation. Detection aims to confirm the presence of nonlinear effects between the system’s input and output [38]. Subsequently, characterization identifies the location, type, and functional form of these nonlinearities [39]. According to the formulation in [4], the functional form can generally be represented by a solution functional (operator) \mathcal{M}_μ parameterized by μ , which maps the system’s input $f(t)$ to its output $y(t)$, expressed as $y(t) = \mathcal{M}_\mu(f(t))$. Building this solution functional relates to forward modeling, and conventional methods heavily rely on physics-based models to have an explicit \mathcal{M}_μ , which can be infeasible if there are unknown mechanisms embedded in complex systems. Also, conventional methods may not work if one opts for customizing the parameters μ . Lastly, parameter estimation [40] involves determining the system coefficients μ , which belongs to inverse modeling. Typical methods include structural model updating [13], restoring force surface method [41], auto-regressive models [42], neural networks [43], etc.

Vibration-based *Structural health monitoring (SHM)* is another typical application in structural dynamics, aiming to identify potential damage of structural systems. Most vibration-based SHM methods can be categorized as either pattern recognition [6, 44] or inverse problem [45]. For pattern recognition-based methods, specific properties (often called damage-sensitive) of response data are extracted and used for damage identification tasks, formulated as novelty detection [46], classification [47], and regression [48], etc. For inverse problem-based methods, which are closely related to parameter estimation, involving determining structural parameters and their changes, which can be related to structural integrity and health [49–51].

The proposed unified framework for modeling structural dynamics can be conveniently adapted to certain tasks of system identification and SHM. Particularly, the forward modeling is equivalent to nonlinearity characterization in system identification, where we employ neural networks to learn a solution operator \mathcal{M}_μ . Additionally, the inverse modeling can estimate the system parameters, which can be user-defined for describing structural state and health.

3. Methodology

3.1. Problem formulation

Consider a *structural dynamic system* defined by the mapping between input and output functions as follows:

$$y(t) = \mathcal{M}_\mu(f(t)), \quad (1)$$

where $\boldsymbol{\mu} = \{\mu_1, \mu_2, \dots\}$ represents a set of parameters that characterize the investigated system; $f(t)$ denotes the excitation force function, and $y(t)$ is the system's dynamic response function; t is the time. The operator $\mathcal{M}_{\boldsymbol{\mu}}$ parametrized by $\boldsymbol{\mu}$ maps the excitation force function to the dynamic response function, which typically involves solving the intrinsic dynamics of the system. For instance, $\mathcal{M}_{\boldsymbol{\mu}}$ can be considered as a Duhamel's integral for a linear single-degree-of-freedom system.

As illustrated in Figure 1, structural dynamics such as oscillators, beams, or blades can be characterized by different classes of parameters, including physical parameters (e.g., stiffness and damping), geometric parameters (e.g., length and width), and non-physical (customized) parameters (e.g., crack damage parameterized via the location and the length of the crack).

For a specific scenario, one may consider a bounded parameter space. Given data samples from the defined parameter space, this work aims to learn structural dynamics via a data-driven method that generalizes effectively across the parameter space.

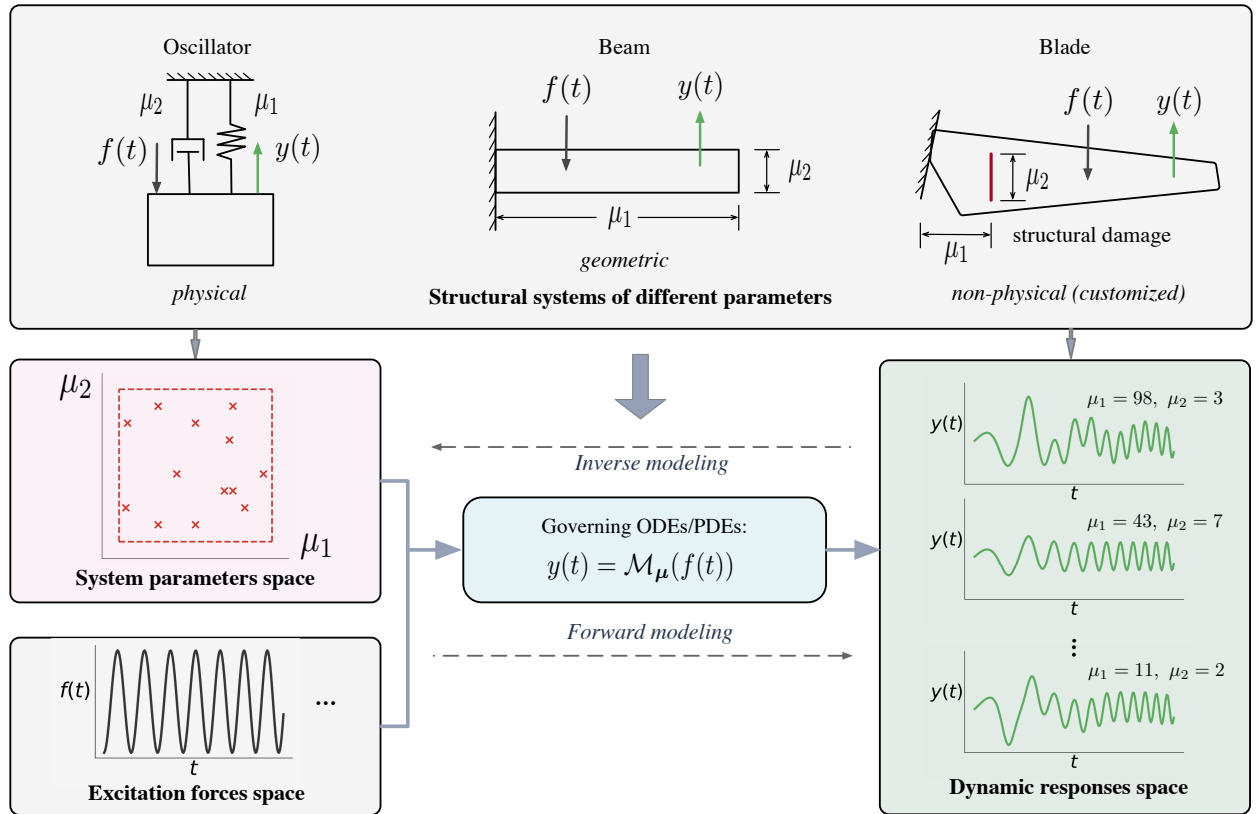


Figure 1: Structural dynamics is defined by the mapping (parameterized by system parameters) from excitation forces to dynamic responses.

The proposed framework is comprised of two major tasks as follows:

- *Forward modeling*: Predicting dynamic response from system parameters and excitation force. We focus on response prediction when system parameters (either physical or non-physical) differ from those in the training data.
- *Inverse modeling*: Estimating system parameters from the pair of dynamic response and excitation force. We aim to directly infer the values of system parameters that were *not* included in the training data.

Although excitation force estimation (force identification) is another case of inverse modeling, it is not considered in our current attempt. The primary objective of this research is to develop a unified data-driven framework that addresses both response prediction (forward modeling) and parameter estimation (inverse modeling) in structural dynamics.

3.2. Neural operators for learning structural dynamics

3.2.1. Vanilla DeepONet

In the setting of vanilla DeepONet [20, 52], two function spaces are considered. Let the input function v 's variable x be defined on the domain $D \subset \mathbb{R}^d$:

$$v : x \mapsto v(x), x \in D, \quad (2)$$

and the output function u 's variable x' be defined on a domain $D' \subset \mathbb{R}^{d'}$:

$$u : x' \mapsto u(x'), x' \in D', \quad (3)$$

where x and x' can be identical or distinct depending on specific applications [53]. Let \mathcal{V} and \mathcal{U} be the function spaces of the input and output functions, respectively. The mapping between the input function v and the output function u is defined by an operator \mathcal{G} :

$$\mathcal{G} : v \in \mathcal{V} \mapsto u \in \mathcal{U}. \quad (4)$$

Given a finite collection of input-output pairs, the motivation of DeepONet is to approximate the true underlying operator via a specially designed neural network architecture. As illustrated in Figure 2a, DeepONet consists of two sub-modules: a branch net B and a trunk net T . The branch net encodes the discretized input function v , accessed at m evaluation points $\{x_1, x_2, \dots, x_m\}$ in D , resulting in $\mathbf{v} = [v(x_1), v(x_2), \dots, v(x_m)]$. The trunk net takes the evaluation points x' in D' as input and outputs $[t_1(x'), t_2(x'), \dots, t_p(x')]$. The forward process of DeepONet is defined as:

$$u(x') = \mathcal{G}(v)(x') \quad (5)$$

$$\approx \sum_{k=1}^p b_k(\mathbf{v}) t_k(x'), \quad (6)$$

where $[b_1, b_2, \dots, b_p]$ and $[t_1, t_2, \dots, t_p]$ are the outputs of the branch net B and trunk net T , respectively. This architecture can be understood as the output function $u(x')$ is learned as the linear combination of basis function $t_k(x')$ via the associated weight $b_k(\mathbf{v})$.

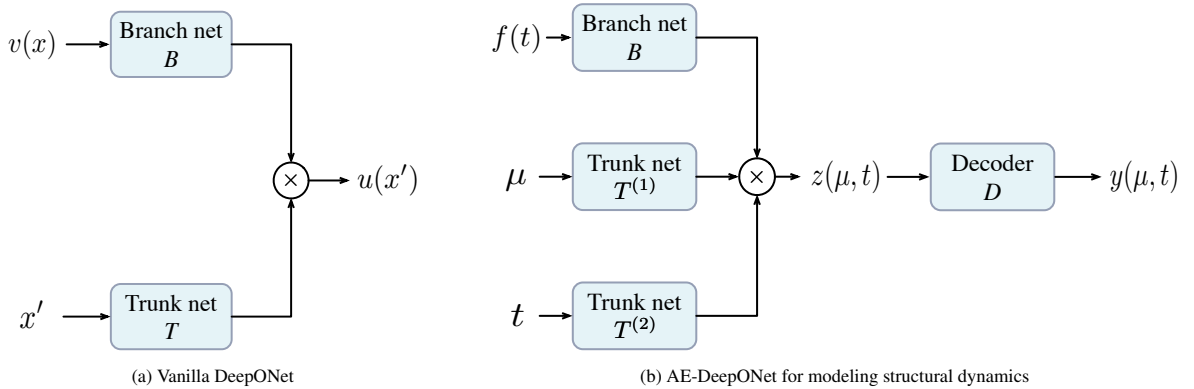


Figure 2: Illustrations of vanilla DeepONet and AE-DeepONet.

3.2.2. Autoencoder-based DeepONet for modeling structural dynamics

To employ the vanilla DeepONet in modeling structural dynamics, the input and output mapping can be considered as:

$$y(t) = \mathcal{G}(f)(t) \approx \sum_{k=1}^p b_k(f) t_k(t), \quad (7)$$

However, applying vanilla DeepONet to model structural dynamics as in Eq.(7) faces two limitations: (1) Vanilla DeepONet has a branch net to encode input functions and a trunk net to encode output evaluation points, while it does not have modules for encoding system parameters $\boldsymbol{\mu}$, making it unsuitable to model parametric structural dynamics formulated in Eq. (1). (2) Vanilla DeepONet is suboptimal for predicting multiple degrees of freedom (DOF) responses based on our empirical implementations. In vanilla DeepONet, the branch net and trunk net are framed as fully connected layers by default. According to our experimental results in Sections 4.2.2 and 4.3.2, fully connected layers are not optimal choices for predicting responses for systems with multiple degrees of freedom.

To address these limitations, we propose the autoencoder-based DeepONet (AE-DeepONet), as illustrated in Figure 2b. AE-DeepONet includes the following enhancements: (1) It includes an additional trunk net to encode system parameters. Inspired by the multiple-input DeepONet [54] and conditioning input mechanism [55], AE-DeepONet has a branch net B , which encodes excitation force function, and two trunk nets $T^{(1)}$ and $T^{(2)}$, which take system parameters and time instances as the evaluation points of the latent space. The process of encoding excitation force, system parameters, and time instances into the latent space is presented as:

$$z(\boldsymbol{\mu}, t) = \mathcal{G}(f)(\boldsymbol{\mu}, t) \quad (8)$$

$$\approx \sum_{k=1}^p b_k(f) t_k^{(1)}(\boldsymbol{\mu}) t_k^{(2)}(t), \quad (9)$$

where $[b_1, b_2, \dots, b_p]$, $[t_1^{(1)}, t_2^{(1)}, \dots, t_p^{(1)}]$ and $[t_1^{(2)}, t_2^{(2)}, \dots, t_p^{(2)}]$ are the outputs of the branch net B , trunk net $T^{(1)}$ and trunk net $T^{(2)}$, respectively; (2) It is flexible for generating response predictions for systems with single- or multi-DOFs. In structural dynamics, it is often necessary to predict responses at different locations. To achieve this, a decoder D is introduced to project the latent state $z(\boldsymbol{\mu}, t)$ to the response space. The decoder can be a convolutional net, which is more suitable for generating multi-channel data, allowing improved performance in the forward modeling.

We term the architecture as autoencoder-based deep operator network (AE-DeepONet): the branch net and the two trunk nets are considered as a whole encoder, and followed by a decoder architecture. Overall, the AE-DeepONet aims to approximate the structural dynamics in Eq. (1) as follows:

$$y(\boldsymbol{\mu}, t) = \mathcal{M}_{\boldsymbol{\mu}}(f(t)) \quad (10)$$

$$\approx \hat{\mathcal{M}}(\boldsymbol{\mu}, f(t)) = D\left(\sum_{k=1}^p b_k(f) t_k^{(1)}(\boldsymbol{\mu}) t_k^{(2)}(t)\right), \quad (11)$$

3.3. A unified framework of forward modeling and inverse modeling

3.3.1. Forward modeling

In forward modeling, a neural operator network, denoted as $\hat{\mathcal{M}}$, is designed to approximate the true forward operator $\mathcal{M}_{\boldsymbol{\mu}}$ in Eq. (1). Specifically, this forward neural network takes the excitation force $f(t)$ and system parameters $\boldsymbol{\mu}$ as input, and outputs the predicted dynamic response $\hat{y}(\boldsymbol{\mu}, t)$, expressed as:

$$\hat{y}(\boldsymbol{\mu}, t) = \hat{\mathcal{M}}(\boldsymbol{\mu}, f(t)). \quad (12)$$

The forward neural network is trained via supervised learning with a training dataset $\mathcal{D}_{\text{train}} = \{s_1, s_2, \dots, s_n\}$, where each data sample $s_i = (f_i(t), \boldsymbol{\mu}_i, y_i(\boldsymbol{\mu}_i, t))$ is a triple of excitation force, system parameters, and dynamic response. In our implementation, we assume the same time resolution and period for excitation force and dynamic response, simplifying each data sample to $s_i = (f_i, \boldsymbol{\mu}_i, y_i)$, with $f_i = f_i(t)$ and $y_i = y_i(\boldsymbol{\mu}_i, t)$. The forward modeling process is as follows:

$$\hat{y} = \hat{\mathcal{M}}(\boldsymbol{\mu}, f). \quad (13)$$

Suppose the forward neural network is parameterized by θ . During the training stage, the parameters of the neural network are optimized as:

$$\hat{\mathcal{M}}^* = \hat{\mathcal{M}}_{\theta^*} = \arg \min_{\theta} \sum_{s_i \in \mathcal{D}_{\text{train}}} \mathcal{L}(\hat{y}_i, y_i), \quad (14)$$

where $\mathcal{L}(\cdot)$ denotes the loss function, and our implementation uses the normalized root mean squared error (NRMSE) (defined in Eq. (19)).

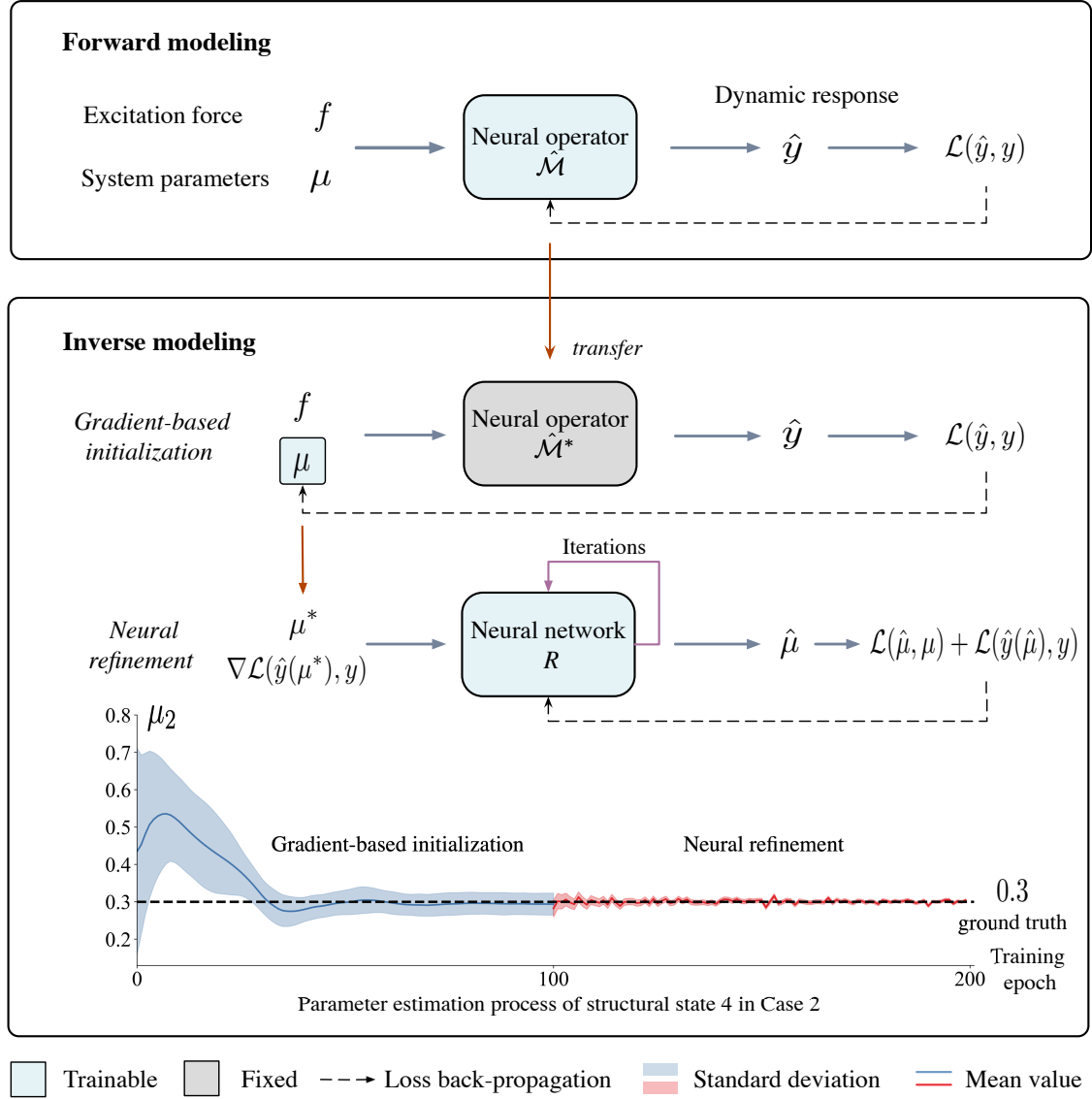


Figure 3: A unified framework for forward and inverse modeling. In forward modeling, a neural network takes excitation force f and system parameter μ as input and predicts dynamic response y . In inverse modeling, gradient-based initialization initializes system parameters μ by minimizing the forward prediction loss given the (f, y) ; subsequent neural refinement employs a neural network to take the initially estimated parameter as input and generates refined parameter estimation results.

3.3.2. Inverse modeling

In inverse modeling, the framework aims to estimate system parameters from pairs of excitation forces and dynamic responses. The parameter estimation involves two steps: *gradient-based initialization* and *neural refinement*. The first step provides an initial estimate of system parameters via forward loss minimization, while the second step refines these estimates by another trainable neural network R to improve the performance.

In gradient-based initialization, we hypothesize that a well-trained neural network $\hat{\mathcal{M}}^*$ in forward modeling can serve as a surrogate model that predicts responses \hat{y} , when system parameters and input force are given:

$$\hat{y} = \hat{\mathcal{M}}^*(\mu, f). \quad (15)$$

To find an optimal system parameter μ^* , a pragmatic way is to minimize the discrepancy between the response prediction \hat{y} and its desired dynamic response y :

$$\mu^* = \arg \min_{\mu} \sum_{(f_i, y_i) \in \mathcal{D}_{\text{train}}} \mathcal{L}(\hat{y}_i, y_i), \quad (16)$$

The parameters of the pre-trained neural network $\hat{\mathcal{M}}^*$ are fixed during inverse modeling. Since the neural network is differentiable with respect to μ , the parameter estimation can be achieved via the gradient-based optimization on the forward prediction loss. μ^* denotes the parameter estimation result with minimized forward prediction loss.

However, estimating system parameters μ solely relying on minimizing forward loss w.r.t $\nabla \mathcal{L}(\hat{y}, y)$ can encounter ill-posed issues due to the non-uniqueness of the solutions. Therefore, the results of gradient-based initialization are often inaccurate, being stuck at local minima. As shown in Figure 3, for the selected example parameter, although the gradient-based initialization process generates satisfactory mean values, the high standard deviation implies the ill-posed problem – choosing different initialization of μ leads to very distinct estimation results, i.e., the estimation is very sensitive to the initialization.

To alleviate this issue, we introduce the *neural refinement* method. A refinement network termed as R , is designed to learn the gradient required for updating system parameters. This approach is inspired by the iterative deep neural networks [56], which have shown effectiveness in mitigating ill-posed problems in tomographic inversion. In the context of parameter estimation, the parameter refinement network takes the initially estimated parameters μ^* from gradient-based initialization, together with the forward loss gradient $\nabla \mathcal{L}(\hat{y}, y)$ as inputs, to iteratively generate learned steps $\Delta \mu$ for updating initially estimates μ^* . This parameter refinement network is implemented as follows:

$$\hat{\mu} = \text{ITERATIVE}(R, \mu^*, \nabla \mathcal{L}(\hat{y}, y)), \quad (17)$$

where $\hat{\mu}$ is the refinement results of parameter estimation, and the $\text{ITERATIVE}(\cdot)$ is an iterative process detailed in lines 14-19 of Algorithm 2.

Suppose the parameter refinement network R is parameterized by β . During the training stage for inverse modeling, not only estimated parameter $\hat{\mu}$ should meet its labeled value μ , but also we demand that the corresponding predicted dynamic response $y(\hat{\mu})$ should match its desired value y . This is optimized as follows:

$$R^* = R_{\beta^*} = \arg \min_{\beta} \sum_{s_i \in \mathcal{D}_{\text{train}}} \mathcal{L}(\hat{\mu}_i, \mu_i) + \mathcal{L}(\hat{y}_i(\hat{\mu}_i), y_i). \quad (18)$$

As illustrated in Figure 3, the neural refinement steadily improves the parameter estimation, as well as reduces the standard deviation of the estimates. This process effectively mitigates the ill-posed problems, leading to more robust and accurate results in inverse parameter estimation.

3.4. Summary

The training processes of forward modeling and inverse modeling are presented in Algorithms 1 and 2, respectively. After training, the test process of forward modeling involves applying the trained forward model $\hat{\mathcal{M}}^*$ to the test data samples, predicting dynamic responses. The test process of inverse modeling proceeds in two steps as: first, gradient-based initialization is applied to the test data samples to obtain the preliminary estimate of the system parameters; second, the trained refinement network R^* can iteratively generate the update steps, and yield the refined estimates as the final parameter estimation results.

Algorithm 1 The Training Process of Forward Modeling

- 1: **Inputs:** Training dataset $\mathcal{D}_{\text{train}} = \{s_i = (f_i, \mu_i, y_i)\}_{i=1}^{N_t}$, forward net $\hat{\mathcal{M}}$
 - 2: **for** epoch = 1 : N **do**
 - 3: **for** data sample $s_i, i = 1 : B$ in data batch **do**
 - 4: Predict dynamic response: $\hat{y}_i = \hat{\mathcal{M}}(\mu_i, f_i)$
 - 5: Compute forward loss: $\mathcal{L}_{\text{forward}} = \sum_{i=1}^B \mathcal{L}(\hat{y}_i, y_i) / B$
 - 6: Update $\hat{\mathcal{M}}$ via gradient descent w.r.t $\nabla \mathcal{L}_{\text{forward}}$
 - 7: Save $\hat{\mathcal{M}}$ with minimized forward prediction loss as $\hat{\mathcal{M}}^*$
-

Algorithm 2 The Training Process of Inverse Modeling

```

1: Inputs: Training dataset  $\mathcal{D}_{\text{train}} = \{s_i = (f_i, \mu_i, y_i)\}_{i=1}^{N_t}$ , trained forward net  $\hat{\mathcal{M}}^*$ , parameter refinement net  $R$ 
2: procedure GRADIENT-BASED INITIALIZATION
3:   for epoch = 1 :  $N$  do
4:     for data sample  $s_i, i = 1 : B$  in data batch do
5:       Sample random system parameters:  $\tilde{\mu}_i \sim U(\mu_{\min}, \mu_{\max})$     $\triangleright U(\mu_{\min}, \mu_{\max})$  is a uniform distribution
6:       Predict dynamic response:  $\hat{y}_i = \hat{\mathcal{M}}^*(\tilde{\mu}_i, f_i)$ 
7:       Compute forward loss:  $\mathcal{L}_{\text{forward}} = \sum_{i=1}^B \mathcal{L}(\hat{y}_i, y_i) / B$ 
8:       Update  $\tilde{\mu}_i$  with gradient descent via forward loss minimization w.r.t  $\nabla \mathcal{L}_{\text{forward}}$ 
9:       Save  $\tilde{\mu}$  with minimized forward loss as  $\mu^*$ 
10: =====
11: procedure NEURAL REFINEMENT
12:   for epoch = 1 :  $N$  do
13:     for data sample  $s_i, i = 1 : B$  in data batch do
14:       procedure ITERATIVE( $R, \mu^*, \nabla \mathcal{L}(\hat{y}, y)$ )
15:         Iteration start:  $\mu_i^0 = \mu_i^*$ 
16:         for refine iteration  $j = 1 : J$  do
17:           Generate an update step:  $\Delta \mu_i^j = R(\mu_i^{j-1}, \mathcal{L}(\hat{y}_i(\mu_i^{j-1}), y_i))$ 
18:           Update parameters:  $\mu_i^j = \mu_i^{j-1} + \Delta \mu_i^j$ 
19:         Output:  $\hat{\mu}_i = \mu_i^J$     $\triangleright$  Iterative refinement results
20:         Compute inverse estimation loss:  $\mathcal{L}_{\text{inverse}} = \sum_{i=1}^B \mathcal{L}(\hat{\mu}_i, \mu_i) / B$ 
21:         Compute forward prediction loss:  $\mathcal{L}_{\text{forward}} = \sum_{i=1}^B \mathcal{L}(\hat{y}_i(\hat{\mu}_i), y_i) / B$ 
22:         Update  $R$  with gradient descent w.r.t  $\nabla(\mathcal{L}_{\text{inverse}} + \mathcal{L}_{\text{forward}})$ 
23:       Save  $R$  with minimized loss as  $R^*$ 

```

4. Experiments

We consider two validation cases to evaluate the effectiveness of the proposed framework: the first case (Case 1) involves a forced Duffing oscillator, which is an illustrative example of a single-degree-of-freedom system with nonlinearity; the second case (Case 2) involves a laboratorial wind turbine blade, an experimental structure with multiple degrees of freedom.

4.1. General setting

The proposed framework is a deep learning-based data-driven method, which requires simulation or real data for supervised training. In each validation case, data samples are prepared as collections of triples (f, μ, \ddot{x}) , consisting of the excitation force f , system parameters μ , and response acceleration \ddot{x} . The normalized root mean squared error (NRMSE) is utilized as loss function and evaluation metric, which is defined as:

$$\text{NRMSE} = \sqrt{\frac{\sum_{i=1}^N \|\hat{y}_i - y_i\|^2}{\sum_{i=1}^N y_i^2}}, \quad (19)$$

where \hat{y}_i and y_i are the predicted and true values, respectively. For comparative analysis, the performance of the proposed framework is compared with the following mainstream deep learning models:

- Vanilla DeepONet: It includes one branch net and one trunk net as introduced in Section 3.2.1. The input of the branch net is the concatenation of excitation force f and system parameters μ , and the input of the trunk net is the evaluation points of dynamics response, which is time instances t . The output is the response acceleration \ddot{x} .

- Multi-layer perceptron (MLP): It maps the input to the output through multiple fully connected layers with non-linear activation functions. The concatenation of excitation force f and system parameters μ is the input of MLP. The response acceleration \ddot{x} is the output of MLP.
- Convolutional neural network (CNN): It consists of several 1D-convolutional and 1D-deconvolutional layers. The convolutional layers map the concatenation of excitation force f and system parameters μ to a latent space, followed by 1D deconvolutional layers mapping the latent space to the response acceleration \ddot{x} .

The module details and parameters of AE-DeepONet and other baseline models are provided in [Appendix B](#) and [Appendix C](#), respectively.

4.2. Case 1 - Duffing oscillator

We first consider a numerical, single-degree-of-freedom system - the Duffing oscillator. The Duffing oscillator [57, 58] is one of the prototype systems in nonlinear dynamics, commonly used for modeling stiffening springs, bulking beams, nonlinear electronic circuits, etc. The governing equation is a second-order, nonlinear ordinary differential equation:

$$\ddot{x}(t) = -\mu_1 x(t) - \mu_2 \dot{x}(t) - \mu_3 x^3(t) + f(t), \quad (20)$$

where μ_1 controls the stiffness; μ_2 controls the damping; μ_3 is the nonlinearity parameter; $f(t)$ is the externally driven (excitation) force; x , \dot{x} , \ddot{x} are the displacement, velocity, and acceleration of the dynamic response, respectively. In this work, the oscillator is considered to be subjected to zero initial conditions, $x(0) = 0$ and $\dot{x}(0) = 0$. For excitation, we consider a sine sweep excitation force with linearly increasing frequency [59], which is defined as:

$$f(t) = A \sin \left(2\pi \left[f_{\text{low}} \cdot t + \frac{(f_{\text{up}} - f_{\text{low}}) \cdot t^2}{2T} \right] \right), \quad (21)$$

where A is the amplitude, f_{low} , f_{up} (in Hz) are the lower and upper limits of the sweep frequency, respectively, and T is the total duration of the excitation.

4.2.1. Parametrization

In this case, we parameterize the Duffing oscillator by stiffness μ_1 and damping μ_2 – only two parameters for the reason of more intuitive visualization to illustrate the framework. Thus, the system parameters are two-dimensional physical parameters, denoted as $\mu = (\mu_1, \mu_2)$. To comprehensively evaluate the generalization performance, we design four cases of increasing complexity (Case 1a - Case 1d), where the system parameters for training and testing include interpolation and extrapolation scenarios. It is noted that most data-driven methods focus on the *interpolation* cases, while *extrapolation* cases are less explored. Figure 4 shows the parameter ranges for each case, detailed as follows:

- *Case 1a*: This is an *interpolation* case; system parameters are sampled from the bounded domain for training and testing. The stiffness μ_1 ranges from [10, 100] and the damping μ_2 ranges from [1, 10].
- *Case 1b*: This case involves *extrapolation*, where the system parameters in the training dataset cover some limited subdomains within the bounded range. The stiffness μ_1 is in range [10, 40] \cup [70, 100] and the damping μ_2 is in range [1, 4] \cup [7, 10].
- *Case 1c*: This case involves *extrapolation*, where the system parameters in the training dataset cover the disjoint subdomains (compared to Case 1b) within the bounded range. The stiffness μ_1 ranges from [10, 100] and the damping μ_2 ranges from [1, 10].
- *Case 1d*: Another *extrapolation* case, where the system parameters for training are confined to a more central subdomain. The stiffness μ_1 ranges from [25, 85] and the damping μ_2 ranges from [2.5, 8.5].

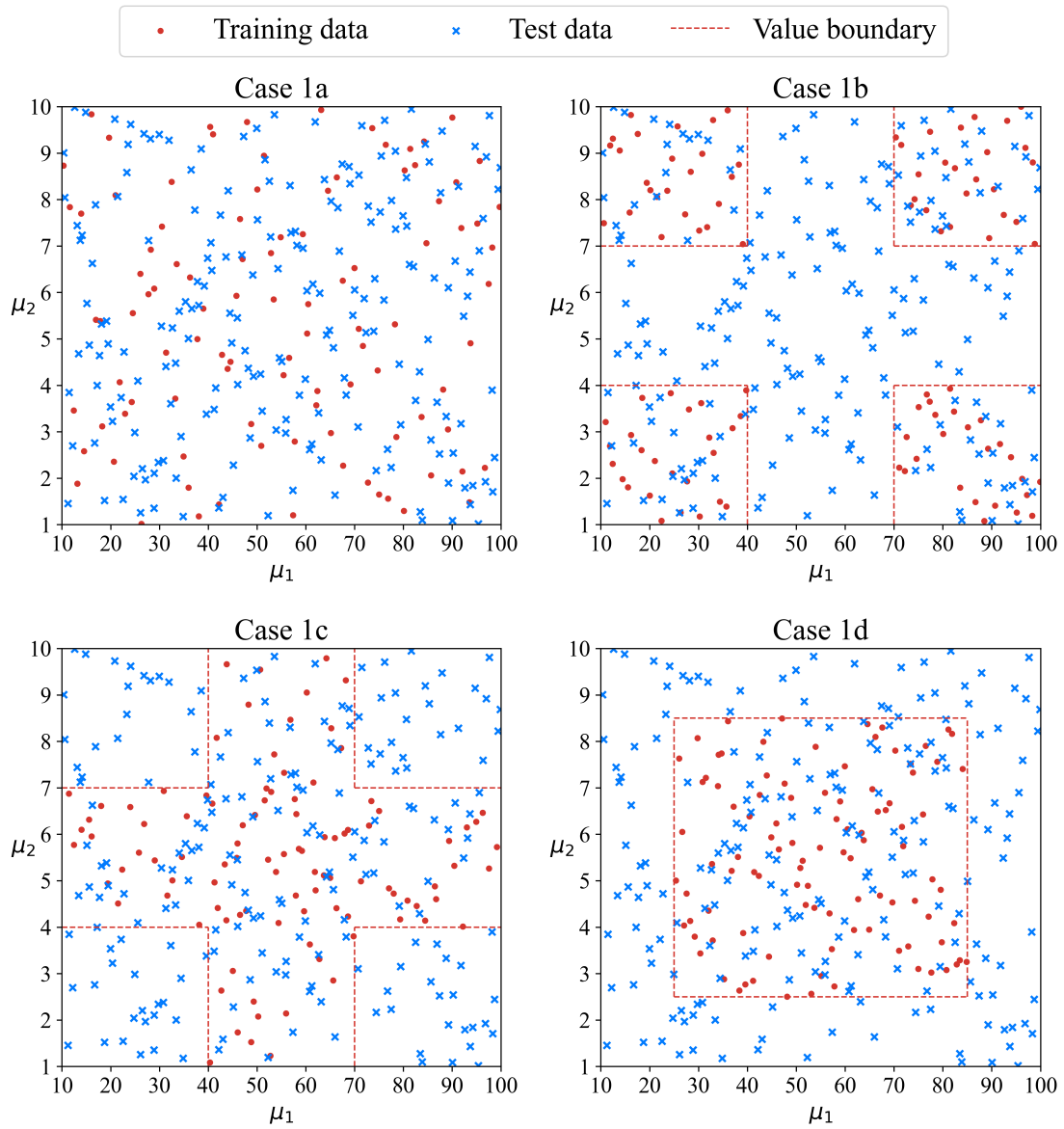


Figure 4: Ranges of system parameters of training and test data in Case 1 (μ_1 is the stiffness, μ_2 is the damping).

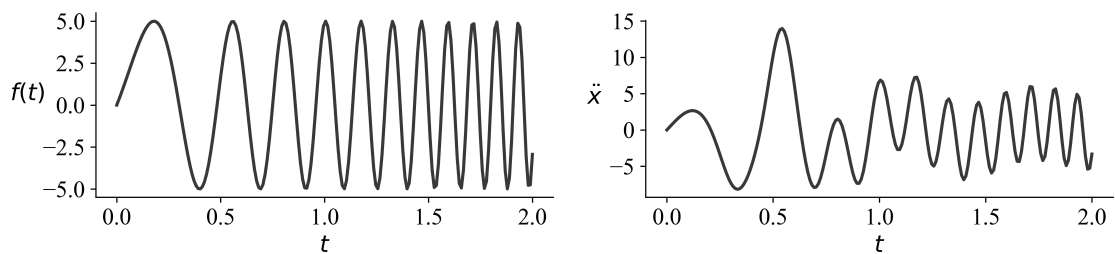


Figure 5: A data sample in Case 1. Left: the excitation force; Right: the response acceleration.

For dataset preparation, the system parameters $\mu = (\mu_1, \mu_2)$ are generated by Latin hypercube sampling method [60], based on the ranges defined in Cases 1a-1d. The nonlinear parameter μ_3 is set to 1×10^4 in all sub-cases. Figure 4 visualizes the distribution of training and test data, which consist of 100 and 200 data samples, respectively. In addition, the test data remains the same across Cases 1a-1d to allow for a fair comparison of generalization performances.

For a data sample, the response acceleration is generated through numerical simulation of the ODE defined in Eq. (20) by the `scipy` package and the `odeint` function in Python. The excitation force $f(t)$ in Eq. (21) is with $A = 5$, $(f_{\text{low}}, f_{\text{up}}) = (1, 10)$ Hz. The excitation force $f(t)$ and response acceleration $\ddot{x}(t)$ are simulated for a duration of $T = 2$ seconds with the time step $\Delta t = 0.01$ seconds, resulting in a length of 200 for both excitation and response. Thus, each data sample is a triple of (f, μ, \ddot{x}) with $f \in \mathbb{R}^{200 \times 1}$, $\mu \in \mathbb{R}^2$ and $\ddot{x} \in \mathbb{R}^{200 \times 1}$. Figure 5 shows the excitation force and the response acceleration of a selected data sample.

4.2.2. Forward modeling results

Table 1 presents the quantitative results of the response prediction of different models in Case 1. In all cases, AE-DeepONet achieves the best response prediction performance across Cases 1a-1d, in terms of NRMSE. DeepONet and MLP are effective in forward modeling as well, with the second- or third-best performance. The CNN exhibits the highest NRMSE, indicating that it is less effective for forward modeling of the Duffing oscillator.

Table 1: NRMSE of response prediction on the **test** dataset of Case 1, for different cases and models.

Case	AE-DeepONet	DeepONet	MLP	CNN
Case 1a	2.66×10^{-2}	6.32×10^{-2}	3.97×10^{-2}	30.34×10^{-2}
Case 1b	2.61×10^{-2}	6.49×10^{-2}	3.86×10^{-2}	30.42×10^{-2}
Case 1c	17.14×10^{-2}	18.76×10^{-2}	17.92×10^{-2}	30.72×10^{-2}
Case 1d	11.52×10^{-2}	12.65×10^{-2}	14.55×10^{-2}	30.57×10^{-2}

Figure 6 further presents the qualitative results of the response prediction of AE-DeepONet in different cases. In Cases 1a and 1b, the response acceleration of test data samples is very accurately predicted. In Cases 1c and 1d, the response acceleration of the interpolation test data samples is also accurately predicted. The response acceleration of the extrapolation test data samples (the values of the parameter are beyond the bound of training samples) is consistently well predicted, capturing major dynamics albeit with minor errors.

To intuitively explore the framework’s effectiveness in extrapolation, we visualize the latent features z from Eq. (9) (the quantity before the decoder). Since the latent features are high-dimensional, we employ Principle Component Analysis (PCA) to reduce their dimensionality for visualization and better interpretability. Figure 7 presents the first principle component (PC) z_1^{PCA} , plotted against the system parameter μ_1 and μ_2 on the bounded domain. We focus on the first PC because it captures the largest variance in the latent space, making it the most informative element to present how the latent features relate to the system parameters. It is found that $z_1^{\text{PCA}}(\mu_1, \mu_2)$ exhibits a simple and continuous representation, explaining that even if the parameter selection is outside of the training data set, the prediction is reasonable.

4.2.3. Inverse modeling results

Table 2 presents the quantitative results of parameter estimation for different models in Case 1. In Cases 1a and 1b, AE-DeepONet outperforms other models with the lowest NRMSEs. For the stiffness μ_1 , AE-DeepONet achieves the NRMSE of 1.32×10^{-2} and 1.97×10^{-2} in gradient-based initialization for Case 1a and 1b, respectively. After neural refinement, the estimation of μ_1 improves further, with the NRMSE of 1.25×10^{-2} and 1.58×10^{-2} in the same cases. Similarly, for the damping μ_2 , AE-DeepONet achieves the NRMSE of 1.06×10^{-2} and 1.79×10^{-2} in gradient-based initialization for Case 1a and 1b, respectively. After neural refinement, the NRMSE improves to 0.86×10^{-2} and 1.72×10^{-2} , respectively.

In the more challenging extrapolation scenarios of Cases 1c and 1d, AE-DeepONet and DeepONet show similar performance, achieving slightly lower NRMSEs than MLP. However, CNN shows the highest NRMSE in all cases, indicating that it is less effective for parameter estimation of the Duffing oscillator. Additionally, the results in Cases 1c and 1d suggest that without proper gradient-based initialization, neural refinement is unable to improve parameter estimation compared to Cases 1a and 1b.

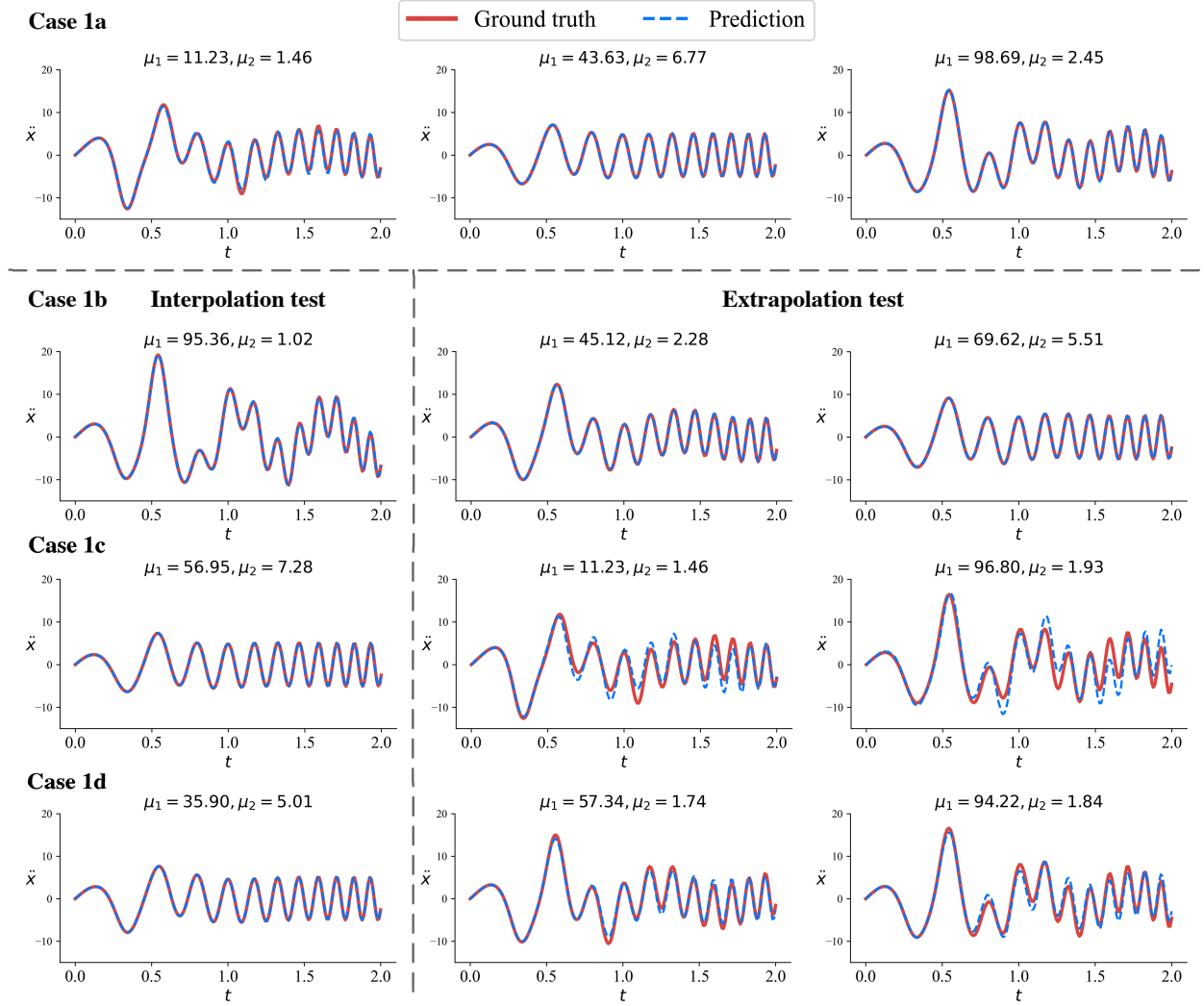


Figure 6: Response prediction results by AE-DeepONet of selected **test** data samples in Case 1 (\ddot{x} in m^2/s , t in 0.01s).

Table 2: NRMSE of parameter estimation of **test** datasets in Case 1, for different cases and models.

Case	AE-DeepONet		DeepONet		MLP		CNN	
	μ_1	μ_2	μ_1	μ_2	μ_1	μ_2	μ_1	μ_2
<i>Gradient-based initialization</i>								
Case 1a	1.32×10^{-2}	1.06×10^{-2}	4.37×10^{-2}	2.28×10^{-2}	2.91×10^{-2}	2.26×10^{-2}	47.52×10^{-2}	48.56×10^{-2}
Case 1b	1.97×10^{-2}	1.79×10^{-2}	3.83×10^{-2}	2.17×10^{-2}	4.61×10^{-2}	5.98×10^{-2}	52.31×10^{-2}	47.91×10^{-2}
Case 1c	7.69×10^{-2}	6.75×10^{-2}	7.59×10^{-2}	6.43×10^{-2}	8.53×10^{-2}	5.27×10^{-2}	47.04×10^{-2}	49.80×10^{-2}
Case 1d	7.57×10^{-2}	4.36×10^{-2}	7.41×10^{-2}	4.30×10^{-2}	7.74×10^{-2}	10.75×10^{-2}	47.67×10^{-2}	49.85×10^{-2}
<i>Neural refinement</i>								
Case 1a	1.25×10^{-2}	0.86×10^{-2}	3.49×10^{-2}	2.72×10^{-2}	2.81×10^{-2}	2.27×10^{-2}	43.04×10^{-2}	47.69×10^{-2}
Case 1b	1.58×10^{-2}	1.72×10^{-2}	3.52×10^{-2}	2.11×10^{-2}	4.39×10^{-2}	5.82×10^{-2}	55.58×10^{-2}	44.24×10^{-2}
Case 1c	7.60×10^{-2}	5.97×10^{-2}	7.36×10^{-2}	5.69×10^{-2}	8.47×10^{-2}	5.44×10^{-2}	44.14×10^{-2}	45.72×10^{-2}
Case 1d	7.42×10^{-2}	4.28×10^{-2}	5.77×10^{-2}	4.56×10^{-2}	8.28×10^{-2}	10.14×10^{-2}	43.45×10^{-2}	43.94×10^{-2}

Figure 8 further presents the qualitative results of AE-DeepONet after neural refinement. In Cases 1a and 1b, both the stiffness and damping are estimated with high accuracy. Notably, Case 1b involves m^2 both inverse modeling

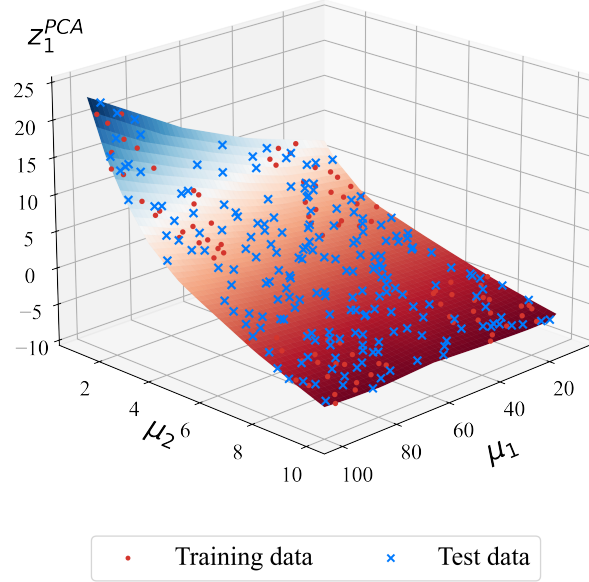


Figure 7: Visualization of the z_1^{PCA} in Case 1b (z_1^{PCA} is the first principle component of the latent features z).

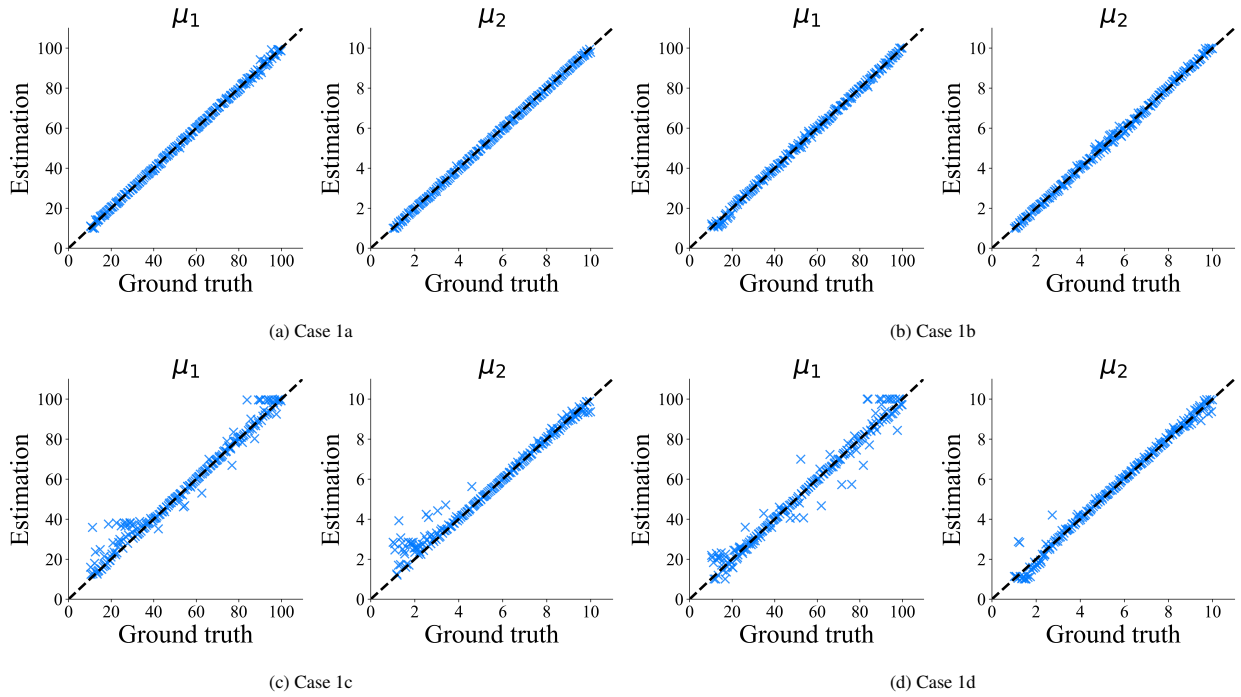


Figure 8: Parameter estimation results of **test** data samples after neural refinement in Case 1 (μ_1 is the stiffness, μ_2 is the damping).

and extrapolation, which is considerably challenging. In more challenging extrapolation cases (Cases 1c and 1d), parameters outside the training range, such as stiffness and damping in Case 1c, and stiffness in Case 1d - are estimated less accurately while still maintained in a reasonable range. For the gradient-based initialization results, the details

are provided in Figure A.15.

Overall, AE-DeepONet, DeepONet, and MLP are effective for parameter estimation of the Duffing oscillator. In interpolation (Case 1a) and mild extrapolation (Case 1b) scenarios, AE-DeepONet exhibits competitive results in inverse modeling. However, all current models still have room for improvements for the strong extrapolation cases (Cases 1c and 1d). Models and methods with better generalization performance are expected to address the challenges posed by strong extrapolation in inverse modeling.

4.3. Case 2: Experimental wind turbine blade

To further validate the proposed framework in more practical scenarios, we consider an experimental wind turbine blade in [61]. The wind turbine blade has a length of 1.75 m and a mass of 5.0 kg. As shown in Figure 10, eight accelerometers are installed on the blade to record its accelerations at different locations, capturing the dynamic responses under the excitation from a shaker. Ten structural healthy states are physically introduced into the wind turbine blade, including one healthy state and nine damaged states (cracks). Specifically, three different damage locations are considered at 17%, 30%, and 50% of the blade length, respectively. In each location, three different damage lengths are considered of 5, 10, 15 cm, respectively. The location and severity of each structural damage are illustrated in Figure 9 and 10.

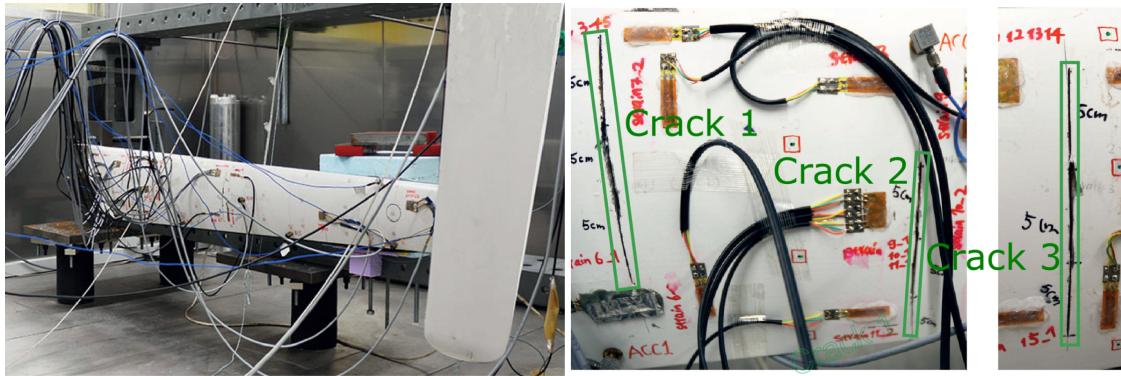


Figure 9: Left: Laboratory configuration, Right: Crack damages. (image credits: Ou, et al. from [61]).

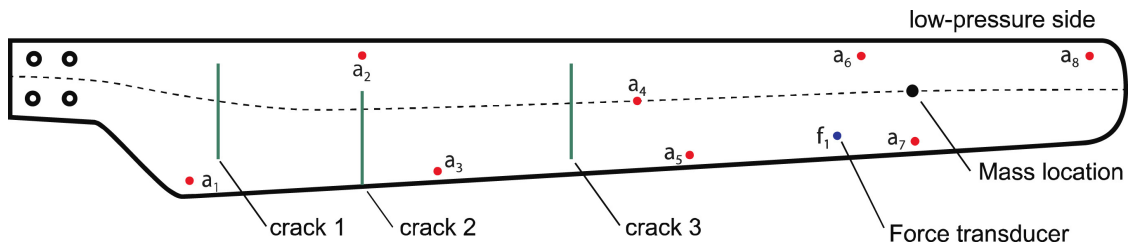
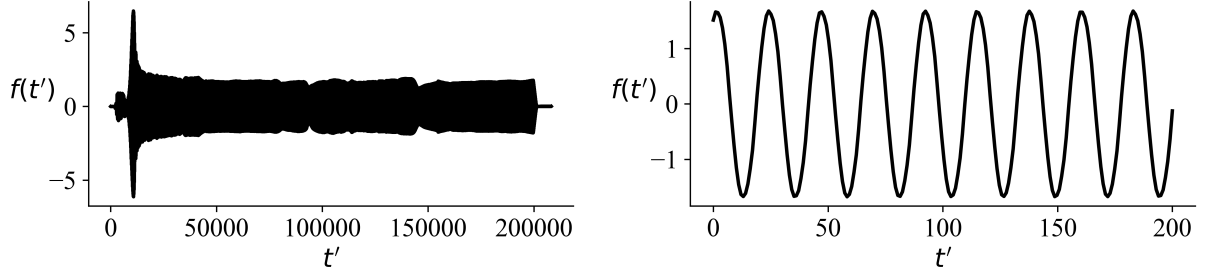


Figure 10: Sensor configuration on the tested wind turbine blade (image credits: Ou, et al. from [61]).

For each structural state, the wind turbine blade is excited by a sine sweep force for around 120 seconds, with frequencies ranging from 1 to 300 Hz. During excitation, both the excitation force and the dynamic response acceleration of the blade are measured with a sampling frequency of 1666 Hz. Figure 11 shows the total excitation period of an experiment, with each excitation having approximately $120 \times 1666 = 199,920$ time instances.

4.3.1. Parameterization

Parameterization refers to identifying the minimal set of parameters that fully characterize a physical system [1]. However, it is often challenging to define a complete set of parameters of complex dynamical systems, particularly in real mechanical or civil structures. In this regard, customizing a handful of parameters relevant to the application



(a) The excitation period of an experiment

(b) The excitation period of a data sample

Figure 11: The sine sweep excitation force in Case 2 (t' is the time instance, $t' = \frac{1}{1666}$ s).

context becomes a pragmatic solution. In this case, we illustrate that the proposed method can be framed for the task of structural damage identification.

In the context of structural health monitoring, damage identification aims to assess structural health at different levels, including damage detection, localization, and quantification [62]. To attain the equivalent goals, we define a six-dimensional parameter $\boldsymbol{\mu} = (\mu_1, \mu_2, \mu_3, \mu_4, \mu_5, \mu_6)$ to describe the structural healthy state of the blade as follows:

- $\boldsymbol{\mu}$ is for damage detection, which indicates the existence of damage.
- $\mu_{\text{Location}} = (\mu_1, \mu_2, \mu_3)$ is for damage localization, which describes the relative locations of cracks 1, 2, and 3.
- $\mu_{\text{Length}} = (\mu_4, \mu_5, \mu_6)$ is for damage quantification, which describes the relative length of cracks 1, 2, and 3.

Specifically, the parameter $\boldsymbol{\mu}$ is normalized as follows:

$$\mu_i = \begin{cases} L_{\text{location}} / L_{\text{length}} & i = 1, 2, 3, \\ L_{\text{crack}} / L_{\text{width}} & i = 4, 5, 6, \end{cases} \quad (22)$$

where $L_{\text{length}} = 1.75$ m and $L_{\text{width}} = 20$ cm are the total length and mean width of the blade, and L_{location} and L_{crack} are the location and length of the structural damages (cracks). It is noted that conventional ideas to quantify the damage are to use physical metrics (such as stiffness reduction), while it is not feasible to directly derive these metrics from the presence of the cracks. As the proposed framework is a data-driven method, it offers the flexibility of customizing the parametrization.

Table 3: Information on structural state and parameterization of the wind turbine blade (States 1,2,3,4,7,10 are used for training; States 5,6,8,9 are used for testing).

State label	Parameterization						Damage location and severity		
	μ_{Location}			μ_{Length}			Crack 1	Crack 2	Crack 3
	μ_1	μ_2	μ_3	μ_4	μ_5	μ_6			
1	0.17	0.3	0.5	0	0	0	healthy		
2	0.17	0.3	0.5	0.25	0	0	5cm	-	-
3	0.17	0.3	0.5	0.25	0.25	0.25	5cm	5cm	-
4	0.17	0.3	0.5	0.25	0.25	0.25	5cm	5cm	5cm
5	0.17	0.3	0.5	0.5	0.25	0.25	10cm	5cm	5cm
6	0.17	0.3	0.5	0.5	0.5	0.25	10cm	10cm	5cm
7	0.17	0.3	0.5	0.5	0.5	0.5	10cm	10cm	10cm
8	0.17	0.3	0.5	0.75	0.5	0.5	15cm	10cm	10cm
9	0.17	0.3	0.5	0.75	0.75	0.5	15cm	15cm	10cm
10	0.17	0.3	0.5	0.75	0.75	0.75	15cm	15cm	15cm

We further use the addition of three 1D-Gaussian functions to encode the parameters into a function:

$$y(x; \mu_1, \mu_2, \mu_3, \mu_4, \mu_5, \mu_6) = \frac{\mu_4}{\sigma \sqrt{2\pi}} \exp\left(\frac{-(x - \mu_1)^2}{2\sigma^2}\right) + \frac{\mu_5}{\sigma \sqrt{2\pi}} \exp\left(\frac{-(x - \mu_2)^2}{2\sigma^2}\right) + \frac{\mu_6}{\sigma \sqrt{2\pi}} \exp\left(\frac{-(x - \mu_3)^2}{2\sigma^2}\right), \quad (23)$$

where $\sigma = 0.01$ is the standard deviation, and $\exp(\cdot)$ is the natural exponential function. Figure 12 shows the qualitative visualization of each structural state, with the horizontal axis representing the relative location of the structural damage and the vertical axis representing the relative length of the structural damage.

For data pre-processing, a low-pass filter with a cut-off frequency of 380 Hz is applied to the raw acceleration measurements. For dataset preparation, data samples are generated by windowing the force and acceleration data between 50,000 to 70,000 time instances in an experiment, with a fixed length of 200 (as shown in Figure 11). Within this period, each structural state is excited under similar external forces. We utilize the acceleration measurements of a_1 to a_4 , whose locations are presented in Figure 10. Each data sample is a triple of (f, μ, \ddot{x}) with $f \in \mathbb{R}^{200 \times 1}$ and $\mu \in \mathbb{R}^6$ and $\ddot{x} \in \mathbb{R}^{200 \times 4}$. The training dataset includes six structural states with state labels 1, 2, 3, 4, 7 and 10, while the test dataset includes four structural states with state labels 5, 6, 8 and 9. Acceleration data of the training and test datasets is normalized to $[-1, 1]$. Each structural state includes 100 data samples for either training or testing. Thus, the training and test datasets include 600 and 400 data samples, respectively.

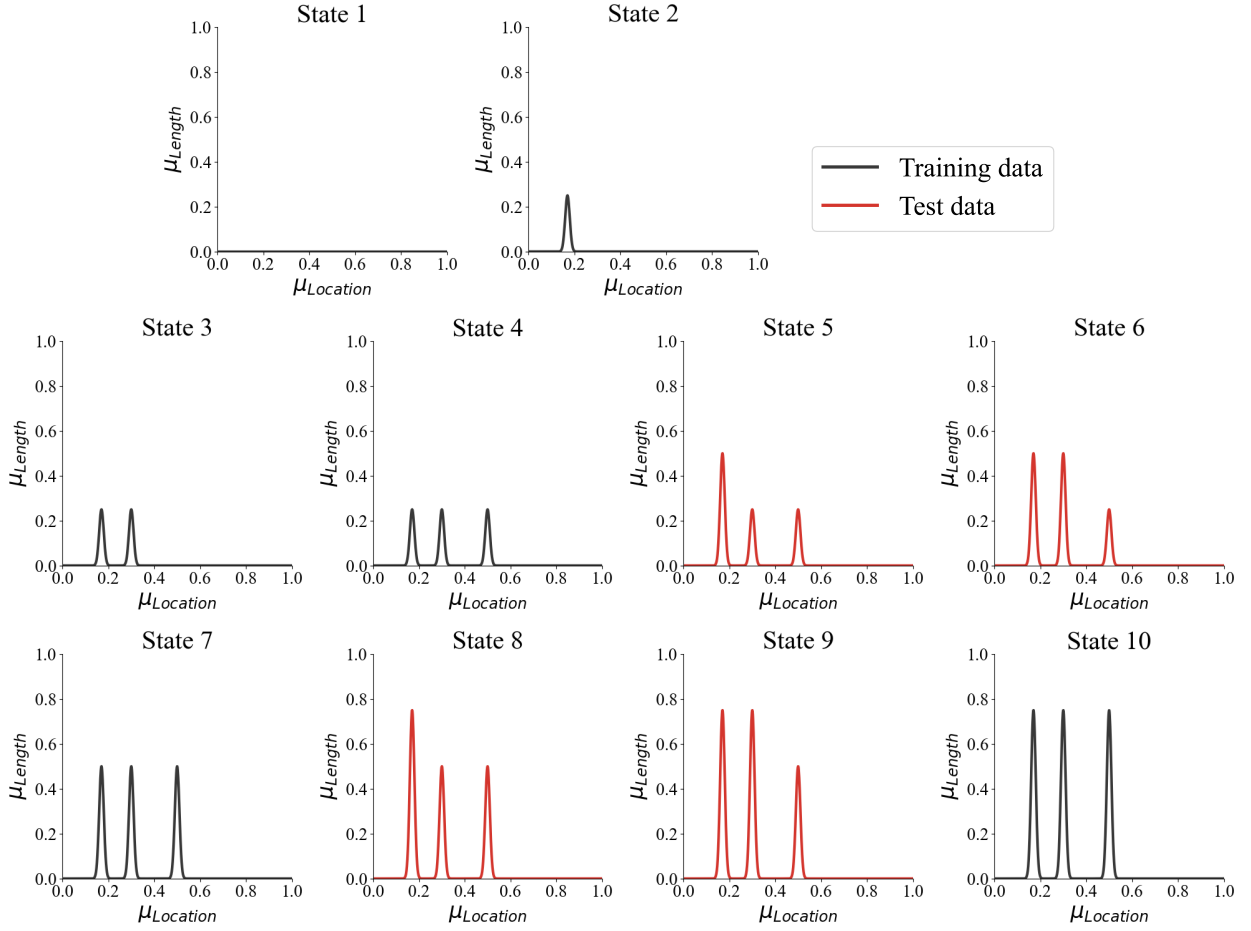


Figure 12: Qualitative visualization of system parameters of the blade, for different structural healthy states. $\mu_{Location}$ and μ_{Length} describe the relative location and length of damage.

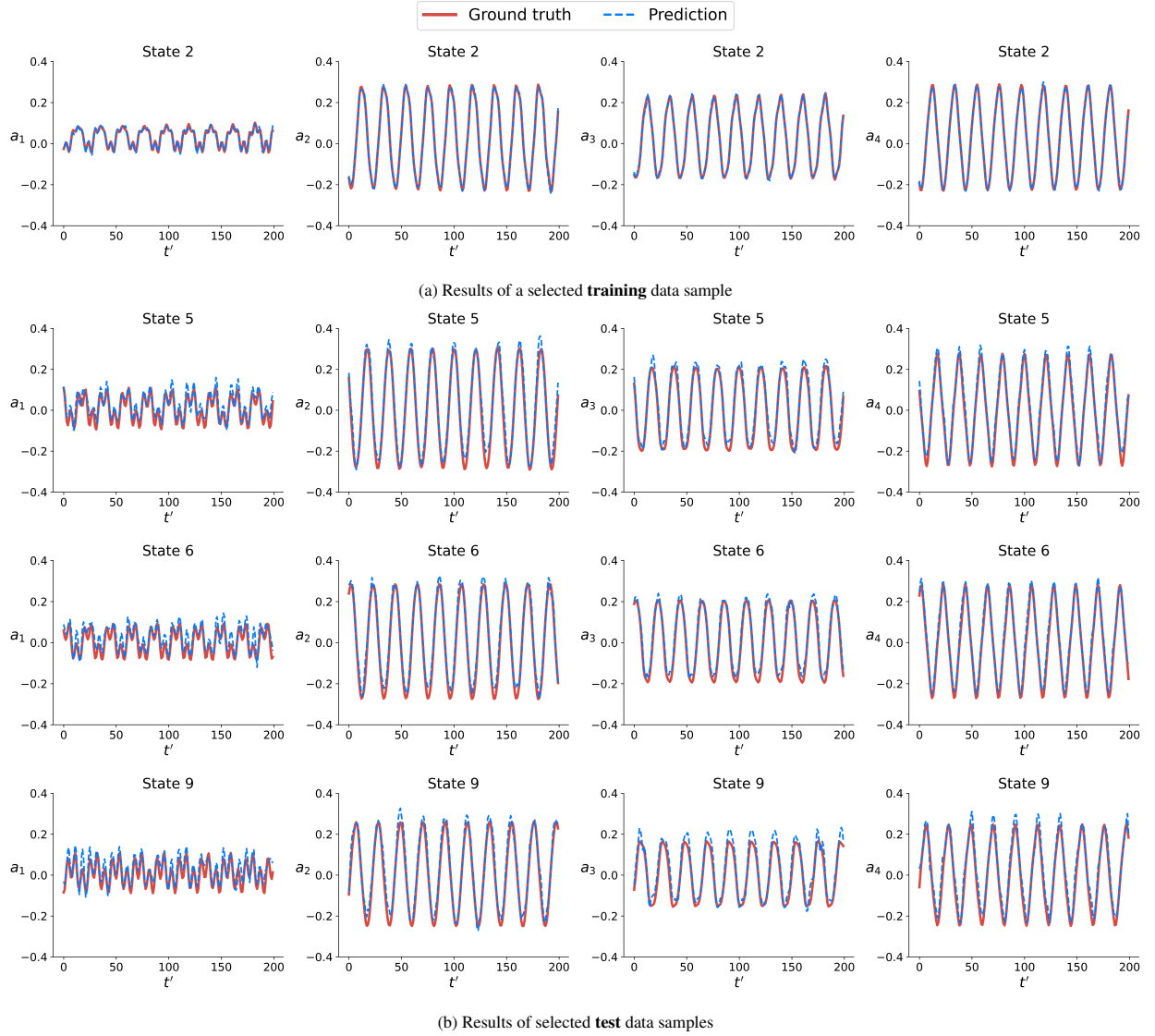


Figure 13: Response prediction results of data samples in Case 2 ($a_1 - a_4$ denote normalized acceleration measurements, t' is the time instances).

4.3.2. Forward modeling results

Table 4 presents the NRMSE for response prediction of different models in Case 2. AE-DeepONet and CNN achieve the best performance on both training and test data. AE-DeepONet achieves the NRMSE of 0.65×10^{-1} on the training data and 2.18×10^{-1} on the test data. CNN follows closely with NRMSE of 0.64×10^{-1} for training and 2.32×10^{-1} for test data. In contrast, DeepONet and MLP perform less effectively in the forward modeling of the wind turbine blade. These models, which are mainly composed of fully connected layers, may struggle to capture the complex dynamics of real structural systems.

Table 4: NRMSE of forward response prediction in the experimental wind turbine blade example, for different datasets and models.

Dataset	AE-DeepONet	DeepONet	MLP	CNN
Training	0.65×10^{-1}	9.91×10^{-1}	1.88×10^{-1}	0.64×10^{-1}
Test	2.18×10^{-1}	10.05×10^{-1}	3.39×10^{-1}	2.32×10^{-1}

Figure 13 presents qualitative results for AE-DeepONet’s response predictions. In particular, Figure 13a shows the response prediction of a selected train data sample, with very high accuracy. Figure 13b shows the response predictions of selected test data samples, where AE-DeepONet successfully captures the major dynamics, though some minor errors remain in local details.

As vanilla DeepONet and MLP demonstrate limitations in modeling such a realistic structural system, AE-DeepONet and CNN generate more accurate response prediction in both training and test data, indicating their robustness and effectiveness with real experimental data. Since excitation force has varying frequencies, the convolution operation in CNN could be more suitable for encoding inputs with different local and global patterns. Therefore, both AE-DeepONet (convolution in branch net) and CNN are effective for the forward modeling of the wind turbine blade.

4.3.3. Inverse modeling results

Table 5: NRMSE of inverse parameter estimation in Case 2, for different datasets and models.

Data	AE-DeepONet		DeepONet		MLP		CNN	
	μ_{Location}	μ_{Length}	μ_{Location}	μ_{Length}	μ_{Location}	μ_{Length}	μ_{Location}	μ_{Length}
<i>Gradient-based initialization</i>								
Training	0.59×10^{-1}	1.33×10^{-1}	10.39×10^{-1}	11.26×10^{-1}	58.82×10^{-1}	57.08×10^{-1}	613.2×10^{-1}	544.1×10^{-1}
Test	1.44×10^{-1}	3.48×10^{-1}	10.45×10^{-1}	8.70×10^{-1}	363.8×10^{-1}	299.6×10^{-1}	735.6×10^{-1}	644.9×10^{-1}
<i>Neural refinement</i>								
Training	0.23×10^{-1}	0.78×10^{-1}	0.80×10^{-1}	4.40×10^{-1}	0.79×10^{-1}	3.57×10^{-1}	0.58×10^{-1}	2.04×10^{-1}
Test	0.54×10^{-1}	3.36×10^{-1}	0.87×10^{-1}	6.90×10^{-1}	0.96×10^{-1}	8.32×10^{-1}	1.16×10^{-1}	3.98×10^{-1}

Table 5 presents the quantitative results of inverse parameter estimation for different models in Case 2. Overall, AE-DeepONet outperforms other baseline models in parameter estimation. For the system parameters μ_{Location} , which describe the relative location of damages, AE-DeepONet achieves the best NEMSE in gradient-based initialization, with the NRMSE of 0.59×10^{-1} on the training data and 1.44×10^{-1} on the test data. After employing neural refinement, the performance further improves, with the NRMSE of 0.23×10^{-1} for training and 0.54×10^{-1} for test data. Similarly, for the system parameters μ_{Length} , which describe the relative length of the damages, AE-DeepONet achieves the best performance in gradient-based initialization, with the NRMSE of 1.33×10^{-1} training data and 3.48×10^{-1} on test data. With neural refinement, the performance improves as well, achieving the NRMSE of 0.78×10^{-1} for training and 3.36×10^{-1} for test data.

Figure 14 presents the qualitative results of AE-DeepONet’s parameter estimation. For structural states 1 and 4, the relative location μ_{Location} and length μ_{Length} of the damage are first estimated by gradient-based initialization, while delivering inconsistent results for the 100 data samples. This is due to the random initialization of the two parameters, and the estimation is sensitive to these initializations. Neural refinement significantly enhances the estimation, with more consistent estimation for all the data samples. One can observe that the estimation is much less dispersive than the former. In State 8, which is not included in the training data and serves as an extrapolation test, similar situations can be concluded, albeit the estimation should be perceived in a statistical way to make more sense. The qualitative parameter estimation results for all structural states are presented in Figure A.16.

In contrast, DeepONet and MLP show less effectiveness in inverse modeling, which could be due to the suboptimal performance in the forward modeling (as shown in Section 4.3.2). AE-DeepONet benefits from a well-trained forward model, enabling better initialization using the gradient-based scheme. The proper initialization of system parameters further contributes to more accurate parameter estimation results after neural refinement. In summary, AE-DeepONet clearly outperforms other baseline models in the inverse parameter estimation. Even in challenging extrapolation test scenarios, AE-DeepONet proves effective in estimating system parameters. Notably, these system parameters are non-physical and customized, being user-defined for the task of structural damage identification. The results indicate the capability of the proposed framework for inverse modeling of the real structural system.

4.4. Implementation details

All experiments are conducted via the Pytorch [63] library on an NVIDIA Geforce RTX 3080 graphic card. For the training process of forward modeling, we set the number of training epochs to 10,000 with a batch size of 64 and a learning rate of 1×10^{-3} . The Adam [64] optimizer is used in Case 1, while the SGD optimizer is used in Case

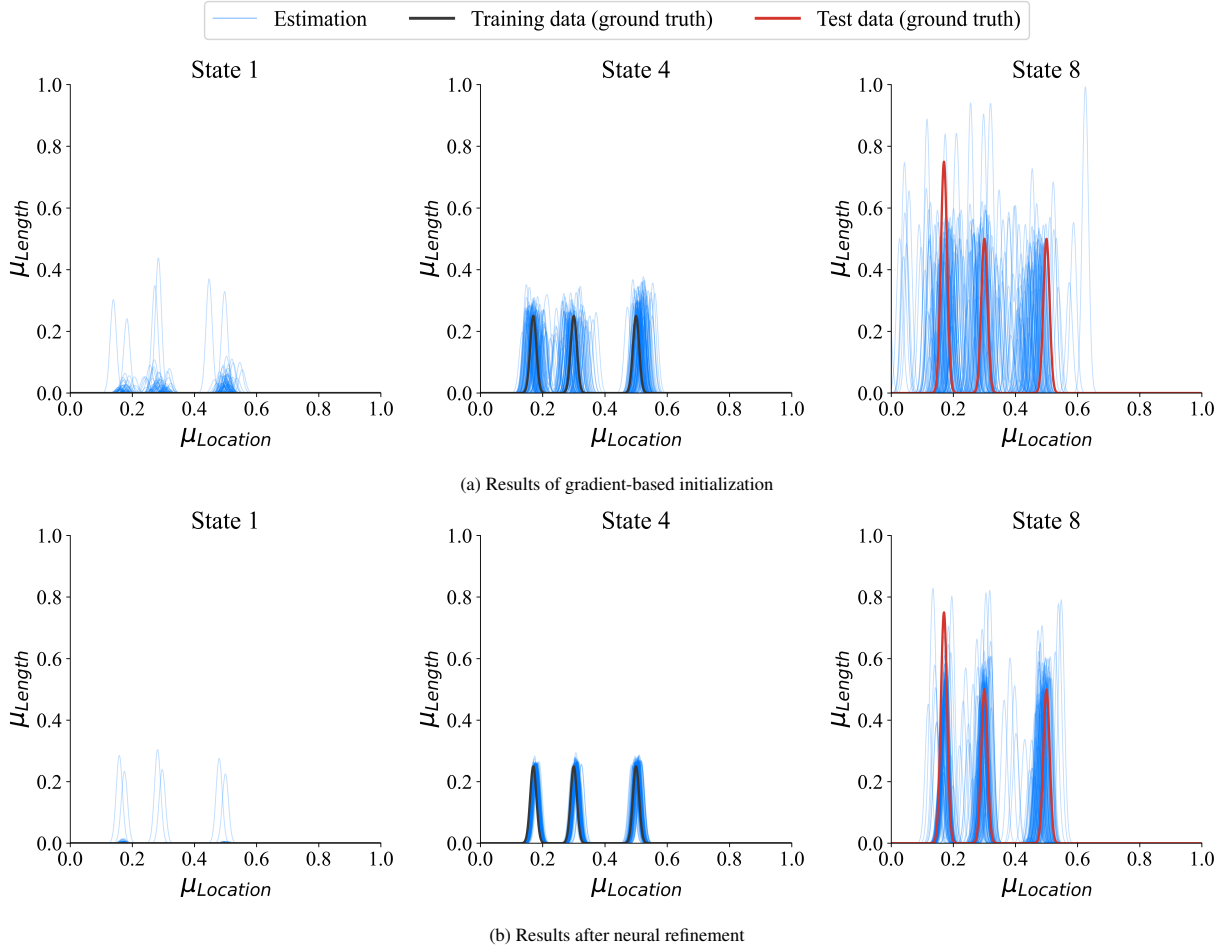


Figure 14: Parameter estimation results of structural states 1, 4, 8 in Case 2.

2. For inverse modeling in Case 1, the training process consists of 5000 epochs for gradient-based initialization and 300 epochs for neural refinement with 1 iteration step. In Case 2, the inverse training process involves 200 epochs for gradient-based initialization and 100 epochs for neural refinement with 3 iteration steps. The neural refinement network in Case 1 is an MLP consisting of 4 layers with input, hidden, and output dimensions of [4, 128, 128, 2], with ReLU activation in hidden layers. The neural refinement network in Case 2 is an MLP consisting of 4 layers with input, hidden, and output dimensions of [12, 256, 256, 6], with ReLU activation in hidden layers.

5. Conclusion

In this work, we present a deep learning-based framework for parameter estimation, which begins by learning a neural operator enabled surrogate model for structural response prediction. The proposed framework offers a unified approach for both forward and inverse problems associated with structural dynamics via neural networks. Within this framework, the autoencoder-based deep neural operator (AE-DeepONet) is proposed to combine parametric input and operator learning. It achieves competitive results in forward modeling and demonstrates significant superiority in inverse problems, boosted by the introduction of neural refinement. The framework is validated through both a simple numerical oscillator and a real experimental wind turbine structure. In our current attempt, we consider the low-dimensional parameter space (up to 7 dimensions in the validation cases), and future work will explore more general settings with high-dimensional parameter spaces. In such cases, dimension reduction techniques are most likely to

be added to the current architecture. Moreover, this framework is architecture-agnostic, with its sub-modules can be easily adaptive to other advanced neural networks like Transformers and graph neural networks, etc. We hope the framework’s performance and flexibility will encourage a new paradigm of addressing inverse problems in structural dynamics by first learning differentiable forward surrogate models via deep learning techniques.

Acknowledgement

The authors wish to express their gratitude for the financial support received from the Guangzhou-HKUST(GZ) Joint Funding Grant (No.2023A03J0105), and the Guangdong Provincial Key Lab of Integrated Communication, Sensing and Computation for Ubiquitous Internet of Things (No.2023B1212010007).

Appendix A. Visualizations

Figure A.15 shows the parameter estimation results of test data samples in Case 1 after gradient-based initialization. In Case 1a-1d, gradient-based initialization is implemented over 5 times on the trained forward model, and the mean values and standard deviations are presented by error bars. Figure A.16 presents the qualitative parameter estimation results in Case 2. The system parameters of ten structural states are estimated via gradient-based initialization and neural refinement.

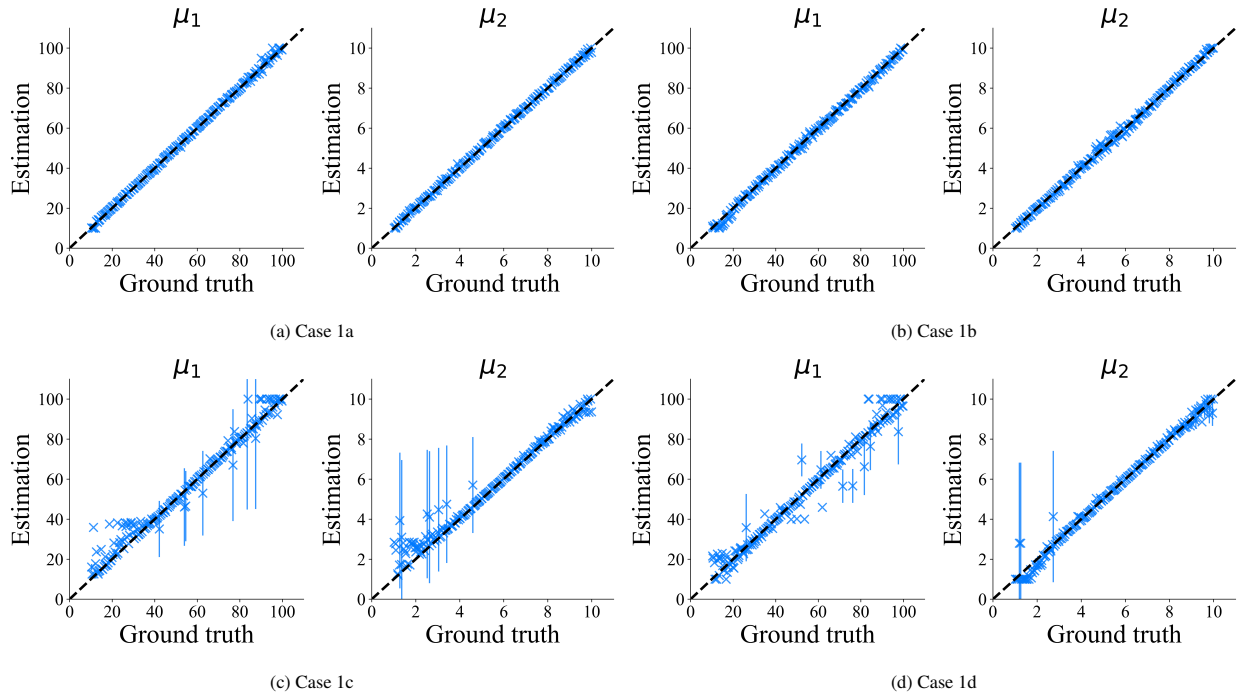


Figure A.15: Parameter estimation results of test data samples in Case 1 after gradient-based initialization (μ_1 is the stiffness, μ_2 is the damping).

Appendix B. Module details of AE-DeepONet

The details of the sub-modules of the AE-DeepONet are as follows:

- Branch net for encoding excitation force: In Case 1, the branch net is a multi-layer perceptron (MLP) consisting of 3 layers with input, hidden, and output dimensions of [200, 256, 256], with rectified linear units (ReLU) activation in hidden layers. In Case 2, the branch net is a 6-layer convolutional neural network (CNN). Each

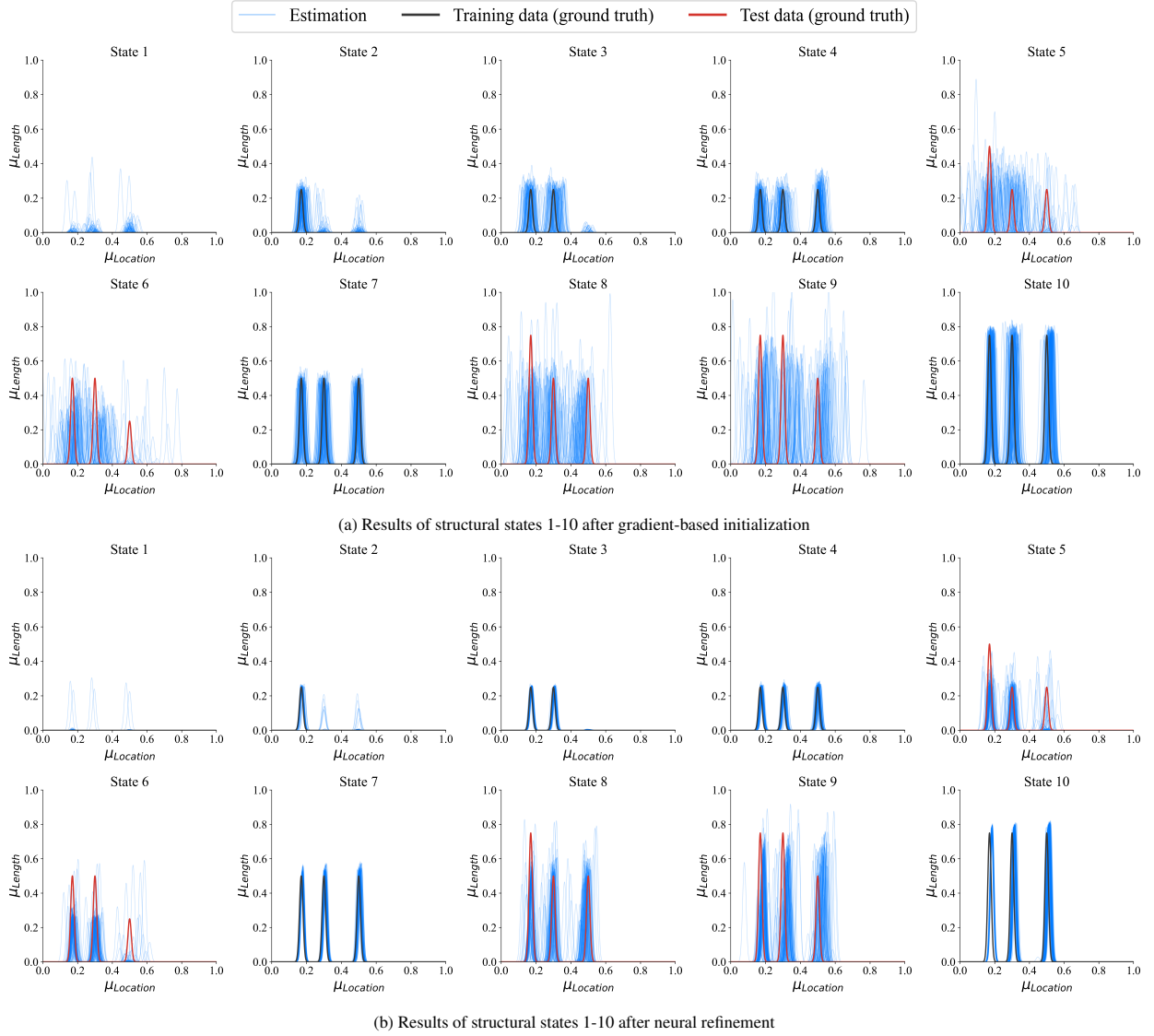


Figure A.16: Qualitative parameter estimation results in Case 2.

layer includes a 1-dimensional convolution (1D-Conv.), batch normalization (BN), and leaky rectified linear units (LeakyReLU) activation. The output channel number is [16, 32, 64, 128, 256, 256], with kernel sizes of [3, 3, 3, 3, 3, 4] and strides of [2, 2, 2, 2, 3, 1], respectively.

- Trunk net for encoding system parameters: In Case 1, the trunk net is a MLP consisting of 3 layers with input, hidden, and output dimensions of [2, 256, 256], with ReLU activation in hidden layers. In Case 2, the trunk net is a MLP consisting of 4 layers with input, hidden, and output dimensions of [6, 300, 300, 256], with ReLU activation in hidden layers.
- Trunk net for encoding time coordinates: In Case 1, the trunk net is a MLP consisting of 3 layers with input, hidden, and output dimensions of [1, 256, 256], with ReLU activation in hidden layers. In Case 2, the trunk net is a MLP consisting of 4 layers with input, hidden, and output dimensions of [200, 300, 300, 256], with ReLU activation in hidden layers.

- Decoder for predicting dynamic response: In Case 1, the decoder is a MLP consisting of 3 layers with input, hidden, and output dimensions of [200, 256, 200], with ReLU activation in hidden layers. In Case 2, the decoder is a deconvolution neural network, which mirrors the CNN-based branch net and consists of 6 layers. Each layer includes a 1-dimensional deconvolution, BN, and LeakyReLU activation. The output channel number is as [256, 128, 64, 32, 16, 4], with kernel sizes [4, 3, 3, 3, 3, 3] and strides of [1, 3, 2, 2, 3, 2], respectively.

Appendix C. Module details of baseline models

For designing the baseline models, we consider that all neural networks have the same hyperparameters and the similar number of parameters to ensure relatively fair comparisons. Table C.6 shows the number of trainable parameters of various models. The implementation and architecture details of the baseline methods are as follows:

- Vanilla DeepONet: In Case 1, the branch net is a MLP of 4 layers with input, hidden, and output dimensions of [202, 300, 300, 300], the trunk net is a MLP of 4 layers with input, hidden, and output dimensions of [1, 300, 300, 300], with ReLU activation in hidden layers. In Case 2, the branch net is a MLP of 5 layers with input, hidden, and output dimensions of [206, 450, 450, 450, 450], the trunk net is a MLP of 5 layers with input, hidden, and output dimensions of [1, 450, 450, 450, 450], with ReLU activation in hidden layers.
- Multi-layer perceptron (MLP): In Case 1, the MLP consists of 5 layers with input, hidden, and output dimensions of [202, 400, 400, 400, 200]. In Case 2, the MLP consists of 6 layers with input, hidden, and output dimensions of [206, 512, 512, 512, 512, 800]. The employed MLPs are with ReLU activation in hidden layers.
- Convolutional neural network (CNN): The CNN has an encoder-decoder architecture consisting of convolutional and deconvolutional layers. Each layer includes convolution or deconvolution operation, BN, and leakyReLU. In Case 1, the encoder consists of 3 convolutional layers, the output channel number is as [64, 128, 512], with kernel sizes 3 and strides 2; the decoder consists of 3 deconvolutional layers, the output channel number is as [128, 64, 1], with kernel sizes 3 and strides 2. In Case 2, the encoder consists of 6 convolutional layers, the output channel number is as [16, 32, 64, 128, 256, 512], with kernel sizes of [3, 3, 3, 3, 3, 4] and strides of [2, 2, 2, 2, 3, 1], respectively; the decoder consists of 6 deconvolutional layers, the output channel number is as [256, 128, 64, 32, 16, 4], with kernel sizes of [4, 3, 3, 3, 3, 3] and strides of [1, 3, 2, 2, 2, 2], respectively.

Table C.6: Number of trainable parameters, for different validation cases and models.

Validation case	AE-DeepONet	DeepONet	MLP	CNN
Case 1	352,969	422,701	482,200	444,417
Case 2	1,185,996	1,304,352	1,682,945	1,313,428

References

- [1] A. Tarantola, Inverse problem theory and methods for model parameter estimation, SIAM, 2005.
- [2] A. Gallet, S. Rigby, T. Tallman, X. Kong, I. Hajirasouliha, A. Liew, D. Liu, L. Chen, A. Hauptmann, D. Smyl, Structural engineering from an inverse problems perspective, *Proceedings of the Royal Society A* 478 (2257) (2022) 20210526.
- [3] J.-P. Noël, G. Kerschen, Nonlinear system identification in structural dynamics: 10 more years of progress, *Mechanical Systems and Signal Processing* 83 (2017) 2–35.
- [4] G. Kerschen, K. Worden, A. F. Vakakis, J.-C. Golinval, Past, present and future of nonlinear system identification in structural dynamics, *Mechanical systems and signal processing* 20 (3) (2006) 505–592.
- [5] C. Zhang, A. A. Mousavi, S. F. Masri, G. Gholipour, K. Yan, X. Li, Vibration feature extraction using signal processing techniques for structural health monitoring: A review, *Mechanical Systems and Signal Processing* 177 (2022) 109175.
- [6] Y. Bao, Z. Chen, S. Wei, Y. Xu, Z. Tang, H. Li, The state of the art of data science and engineering in structural health monitoring, *Engineering* 5 (2) (2019) 234–242.
- [7] S. S. Eshkevari, M. Takáč, S. N. Pakzad, M. Jahani, Dynnet: Physics-based neural architecture design for nonlinear structural response modeling and prediction, *Engineering Structures* 229 (2021) 111582.

- [8] F. Naets, J. Croes, W. Desmet, An online coupled state/input/parameter estimation approach for structural dynamics, *Computer methods in applied mechanics and engineering* 283 (2015) 1167–1188.
- [9] A. B. Abdesslem, N. Dervilis, D. Wagg, K. Worden, Model selection and parameter estimation in structural dynamics using approximate bayesian computation, *Mechanical Systems and Signal Processing* 99 (2018) 306–325.
- [10] R. Liu, E. Dobriban, Z. Hou, K. Qian, Dynamic load identification for mechanical systems: A review, *Archives of Computational Methods in Engineering* 29 (2) (2022) 831–863.
- [11] H. Yang, J. Jiang, G. Chen, J. Zhao, Dynamic load identification based on deep convolution neural network, *Mechanical Systems and Signal Processing* 185 (2023) 109757.
- [12] E. Z. Moore, J. M. Nichols, K. D. Murphy, Model-based shm: Demonstration of identification of a crack in a thin plate using free vibration data, *Mechanical systems and signal processing* 29 (2012) 284–295.
- [13] J. E. Mottershead, M. Friswell, Model updating in structural dynamics: a survey, *Journal of sound and vibration* 167 (2) (1993) 347–375.
- [14] K. Worden, W. J. Staszewski, J. J. Hensman, Natural computing for mechanical systems research: A tutorial overview, *Mechanical Systems and Signal Processing* 25 (1) (2011) 4–111.
- [15] B. Z. Cunha, C. Droz, A.-M. Zine, S. Foulard, M. Ichchou, A review of machine learning methods applied to structural dynamics and vibroacoustic, *Mechanical Systems and Signal Processing* 200 (2023) 110535.
- [16] B. Xu, Z. Wu, G. Chen, K. Yokoyama, Direct identification of structural parameters from dynamic responses with neural networks, *Engineering Applications of Artificial Intelligence* 17 (8) (2004) 931–943.
- [17] X. Lei, D. M. Siringoringo, Z. Sun, Y. Fujino, Displacement response estimation of a cable-stayed bridge subjected to various loading conditions with one-dimensional residual convolutional autoencoder method, *Structural Health Monitoring* 22 (3) (2023) 1790–1806.
- [18] R.-T. Wu, M. R. Jahanshahi, Deep convolutional neural network for structural dynamic response estimation and system identification, *Journal of Engineering Mechanics* 145 (1) (2019) 04018125.
- [19] Z. Lai, W. Liu, X. Jian, K. Bacsá, L. Sun, E. Chatzi, Neural modal ordinary differential equations: Integrating physics-based modeling with neural ordinary differential equations for modeling high-dimensional monitored structures, *Data-Centric Engineering* 3 (2022) e34.
- [20] L. Lu, P. Jin, G. Pang, Z. Zhang, G. E. Karniadakis, Learning nonlinear operators via deepnet based on the universal approximation theorem of operators, *Nature machine intelligence* 3 (3) (2021) 218–229.
- [21] K. Azizzadenesheli, N. Kovachki, Z. Li, M. Liu-Schiaffini, J. Kossaifi, A. Anandkumar, Neural operators for accelerating scientific simulations and design, *Nature Reviews Physics* (2024) 1–9.
- [22] Q. Cao, S. Goswami, G. E. Karniadakis, Laplace neural operator for solving differential equations, *Nature Machine Intelligence* (2024) 1–10.
- [23] Z. Li, N. Kovachki, K. Azizzadenesheli, B. Liu, K. Bhattacharya, A. Stuart, A. Anandkumar, Fourier neural operator for parametric partial differential equations, *arXiv preprint arXiv:2010.08895* (2020).
- [24] J. He, X. Liu, J. Xu, Mgno: Efficient parameterization of linear operators via multigrid, *arXiv preprint arXiv:2310.19809* (2023).
- [25] M. Lu, A. Mohammadi, Z. Meng, X. Meng, G. Li, Z. Li, Deep neural operator for learning transient response of interpenetrating phase composites subject to dynamic loading, *Computational Mechanics* 72 (3) (2023) 563–576.
- [26] G. Lin, C. Moya, Z. Zhang, Learning the dynamical response of nonlinear non-autonomous dynamical systems with deep operator neural networks, *Engineering Applications of Artificial Intelligence* 125 (2023) 106689.
- [27] D. A. Najera-Flores, M. D. Todd, A structure-preserving neural differential operator with embedded hamiltonian constraints for modeling structural dynamics, *Computational Mechanics* 72 (2) (2023) 241–252.
- [28] T. Wu, T. Maruyama, L. Wei, T. Zhang, Y. Du, G. Iaccarino, J. Leskovec, Compositional generative inverse design, *arXiv preprint arXiv:2401.13171* (2024).
- [29] K. Allen, T. Lopez-Guevara, K. L. Stachenfeld, A. Sanchez Gonzalez, P. Battaglia, J. B. Hamrick, T. Pfaff, Inverse design for fluid-structure interactions using graph network simulators, *Advances in Neural Information Processing Systems* 35 (2022) 13759–13774.
- [30] T. Gaskin, G. A. Pavliotis, M. Girolami, Neural parameter calibration for large-scale multiagent models, *Proceedings of the National Academy of Sciences* 120 (7) (2023) e2216415120.
- [31] J. N. Kutz, Machine learning for parameter estimation, *Proceedings of the National Academy of Sciences* 120 (12) (2023) e2300990120.
- [32] M. Takamoto, T. Praditia, R. Leiteritz, D. MacKinlay, F. Alesiani, D. Pflüger, M. Niepert, Pdebench: An extensive benchmark for scientific machine learning, *Advances in Neural Information Processing Systems* 35 (2022) 1596–1611.
- [33] D. MacKinlay, D. Pagendam, P. M. Kuhnert, T. Cui, D. Robertson, S. Janardhanan, Model inversion for spatio-temporal processes using the fourier neural operator, in: *Neurips Workshop on Machine Learning for the Physical Sciences*, 2021, p. 7.
- [34] T. Chen, H. Chen, Universal approximation to nonlinear operators by neural networks with arbitrary activation functions and its application to dynamical systems, *IEEE transactions on neural networks* 6 (4) (1995) 911–917.
- [35] Z. Li, N. Kovachki, K. Azizzadenesheli, B. Liu, K. Bhattacharya, A. Stuart, A. Anandkumar, Neural operator: Graph kernel network for partial differential equations, *arXiv preprint arXiv:2003.03485* (2020).
- [36] S. Garg, H. Gupta, S. Chakraborty, Assessment of deepnet for time dependent reliability analysis of dynamical systems subjected to stochastic loading, *Engineering Structures* 270 (2022) 114811.
- [37] Q. Cao, S. Goswami, T. Tripura, S. Chakraborty, G. E. Karniadakis, Deep neural operators can predict the real-time response of floating offshore structures under irregular waves, *Computers & Structures* 291 (2024) 107228.
- [38] R. J. Allemang, D. Adams, Survey of nonlinear detection and identification techniques for experimental vibrations, in: *Proc. ISMA*, Vol. 23, Citeseer, 1998, pp. 269–281.
- [39] R. Lin, D. Ewins, Location of localised stiffness non-linearity using measured modal data, *Mechanical systems and signal processing* 9 (3) (1995) 329–339.
- [40] A. Poulimenos, S. Fassois, Parametric time-domain methods for non-stationary random vibration modelling and analysis—a critical survey and comparison, *Mechanical systems and signal processing* 20 (4) (2006) 763–816.
- [41] T. J. Rogers, T. Friis, A latent restoring force approach to nonlinear system identification, *Mechanical Systems and Signal Processing* 180 (2022) 109426.
- [42] S. A. Billings, *Nonlinear system identification: NARMAX methods in the time, frequency, and spatio-temporal domains*, John Wiley & Sons,

2013.

- [43] Z. Lai, C. Mylonas, S. Nagarajaiah, E. Chatzi, Structural identification with physics-informed neural ordinary differential equations, *Journal of Sound and Vibration* 508 (2021) 116196.
- [44] C. R. Farrar, K. Worden, *Structural health monitoring: a machine learning perspective*, John Wiley & Sons, 2012.
- [45] M. I. Friswell, Damage identification using inverse methods, *Philosophical Transactions of the Royal Society A: Mathematical, Physical and Engineering Sciences* 365 (1851) (2007) 393–410.
- [46] M. H. Soleimani-Babakamali, R. Sepasdar, K. Nasrollahzadeh, I. Lourentzou, R. Sarlo, Toward a general unsupervised novelty detection framework in structural health monitoring, *Computer-Aided Civil and Infrastructure Engineering* 37 (9) (2022) 1128–1145.
- [47] M. Zhou, Z. Lai, Structural damage classification under varying environmental conditions and unknown classes via open set domain adaptation, *Mechanical Systems and Signal Processing* 218 (2024) 111561.
- [48] S. G. Shahidi, M. B. Nigro, S. N. Pakzad, Y. Pan, Structural damage detection and localisation using multivariate regression models and two-sample control statistics, *Structure and Infrastructure Engineering* 11 (10) (2015) 1277–1293.
- [49] M. Spiridonakos, S. Fassois, Parametric identification of a time-varying structure based on vector vibration response measurements, *Mechanical Systems and Signal Processing* 23 (6) (2009) 2029–2048.
- [50] H. Ebrahimian, R. Astroza, J. P. Conte, C. Papadimitriou, Bayesian optimal estimation for output-only nonlinear system and damage identification of civil structures, *Structural Control and Health Monitoring* 25 (4) (2018) e2128.
- [51] A. H. M. Rubaiyat, D. H. Thai, J. M. Nichols, M. N. Hutchinson, S. P. Wallen, C. J. Naify, N. Geib, M. R. Haberman, G. K. Rohde, Data-driven identification of parametric governing equations of dynamical systems using the signed cumulative distribution transform, *Computer Methods in Applied Mechanics and Engineering* 422 (2024) 116822.
- [52] M. Zhu, H. Zhang, A. Jiao, G. E. Karniadakis, L. Lu, Reliable extrapolation of deep neural operators informed by physics or sparse observations, *Computer Methods in Applied Mechanics and Engineering* 412 (2023) 116064.
- [53] L. Lu, X. Meng, S. Cai, Z. Mao, S. Goswami, Z. Zhang, G. E. Karniadakis, A comprehensive and fair comparison of two neural operators (with practical extensions) based on fair data, *Computer Methods in Applied Mechanics and Engineering* 393 (2022) 114778.
- [54] P. Jin, S. Meng, L. Lu, Mionet: Learning multiple-input operators via tensor product, *SIAM Journal on Scientific Computing* 44 (6) (2022) A3490–A3514.
- [55] V. Dumoulin, E. Perez, N. Schucher, F. Strub, H. d. Vries, A. Courville, Y. Bengio, Feature-wise transformations, *Distill*<https://distill.pub/2018/feature-wise-transformations> (2018). doi:10.23915/distill.00011.
- [56] J. Adler, O. Öktem, Solving ill-posed inverse problems using iterative deep neural networks, *Inverse Problems* 33 (12) (2017) 124007.
- [57] I. Kovacic, M. J. Brennan, *The Duffing equation: nonlinear oscillators and their behaviour*, John Wiley & Sons, 2011.
- [58] G. Duffing, *Erzwungene Schwingungen bei veränderlicher Eigenfrequenz und ihre technische Bedeutung*, no. 41-42, Vieweg, 1918.
- [59] A. Farina, Simultaneous measurement of impulse response and distortion with a swept-sine technique, in: *Audio engineering society convention 108*, Audio Engineering Society, 2000.
- [60] M. D. McKay, R. J. Beckman, W. J. Conover, A comparison of three methods for selecting values of input variables in the analysis of output from a computer code, *Technometrics* 42 (1) (2000) 55–61.
- [61] Y. Ou, K. E. Tatsis, V. K. Dertimanis, M. D. Spiridonakos, E. N. Chatzi, Vibration-based monitoring of a small-scale wind turbine blade under varying climate conditions. part i: An experimental benchmark, *Structural Control and Health Monitoring* 28 (6) (2021) e2660.
- [62] A. Rytter, *Vibrational based inspection of civil engineering structures* (1993).
- [63] A. Paszke, S. Gross, F. Massa, A. Lerer, J. Bradbury, G. Chanan, T. Killeen, Z. Lin, N. Gimelshein, L. Antiga, et al., Pytorch: An imperative style, high-performance deep learning library, *Advances in neural information processing systems* 32 (2019).
- [64] D. P. Kingma, Adam: A method for stochastic optimization, *arXiv preprint arXiv:1412.6980* (2014).